Diabetes, Metabolic Syndrome and Obesity

Dovepress
Taylor & Francis Group

Open Access Full Text Article

ORIGINAL RESEARCH

Mechanisms of Dangguiliuhuang Tang in Streptozotocin-Induced Type 2 Diabetes Mellitus Mice Based on Network Pharmacology, Gut Microbiota, and Experimental Validation

Xianglong Meng[1–4,*], Zhulin Bu[1–4,*], Xiaofen Li[1–4], Jing Ren[1–4], Yuting Dai[1–4], Shuosheng Zhang[1–4]

[1]College of Chinese Materia Medica and Food Engineering, Shanxi University of Chinese Medicine, Jinzhong, Shanxi, People's Republic of China; [2]Key Laboratory of Traditional Chinese Medicine Processing in Shanxi Province, Jinzhong, Shanxi, People's Republic of China; [3]Traditional Chinese Medicine Processing Techniques Heritage Base, Jinzhong, Shanxi, People's Republic of China; [4]Research Laboratory of Traditional Chinese Medicine Processing, Inheritance and Innovation, Jinzhong, Shanxi, People's Republic of China

*These authors contributed equally to this work

Correspondence: Xianglong Meng, Email sszywzh@126.com

Background: Dangguiliuhuang Tang (DGLHT), a classic traditional Chinese medicine formula, has long been used to treat type 2 diabetes mellitus (T2DM). Nevertheless, its therapeutic efficacy, pharmacological foundation, and underlying mechanisms warrant further scientific exploration.

Methods: Ultra-high-performance liquid chromatography coupled with Thermo Vanquish UHPLC-Thermo Q Exactive HFX (UHPLC-QE-MS) was utilized to identify the chemical components of DGLHT. A potential therapeutic network for DGLHT in treating T2DM was constructed using network pharmacology. Untargeted metabolomics techniques were applied to reveal the differential effects of DGLHT on T2DM, and 16S rDNA amplification sequencing technology was used to investigate the differential metabolic regulation of gut microbiota in T2DM mice treated with DGLHT. Molecular biomedical experimental methods were combined to validate and analyze expression levels of the relevant proteins in the liver. A correlation analysis between the active ingredients of DGLHT and the differential gut microbiota was established.

Results: DGLHT improved glycemia, glucose tolerance, and liver injury in T2DM mice. A total of 38 major components were identified. Core targets included mitogen-activated protein kinase 1 (MAPK1), mitogen-activated protein kinase 3 (MAPK3), non-receptor tyrosine kinase (TNK), C-X-C motif chemokine ligand 8 (CXCL8), and serine/threonine kinase 1 (AKT1). DGLHT significantly altered the serum metabolic profile and gut microbiota composition in T2DM mice. These alterations affected inflammation-related Toll-like receptor signaling pathways, phosphorylation-associated ErbB signaling pathways, and functional substance metabolism related to bile secretion, cholesterol metabolism, biosynthesis of unsaturated fatty acids, protein digestion and absorption, cysteine and methionine metabolism, carbohydrate metabolism, intestinal membrane transport, and amino acid metabolism. DGLHT modulated protein expression in several key signaling pathways, including the toll-like receptor 4 (TLR4)/nuclear factor kappa-B (NF-κB)/NOD-like receptor thermal protein domain-associated protein 3 (NLRP3) pathway, phosphatidylinositide 3-kinase (PI3K)/protein kinase B (AKT)/glucose transporter type 4 (GLUT4) pathway, AMP-activated protein kinase (AMPK)/sirtuin 1 (SIRT1)/peroxisome proliferators-activated receptor γ coactivator 1 alpha (PGC-1α) pathway, and heme oxygenase 1 (HO-1)/superoxide dismutase (SOD2)/catalase (CAT) pathway. The Candida genus and gamma-linolenic acid exhibited the strongest correlation.

Conclusion: DGLHT alleviates T2DM insulin resistance via multi-pathway regulation of inflammation, energy metabolism, and oxidative stress, mediated through metabolic and gut microbiota modulation.

Keywords: DGLHT, metabolism, mechanism, multi-omics

Received: 21 March 2025
Accepted: 20 September 2025
Published: 22 October 2025

Graphical Abstract

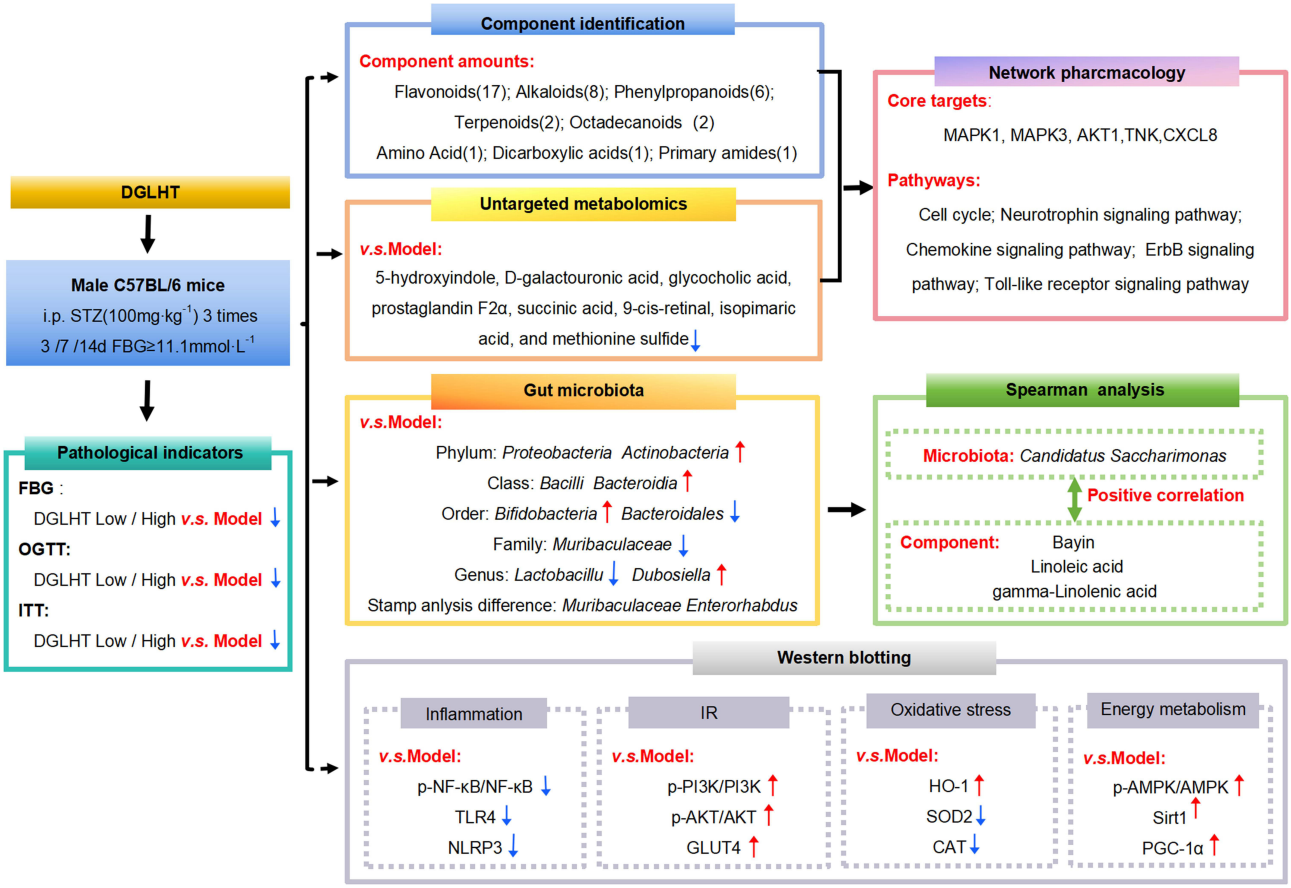

Introduction

Diabetes mellitus is a chronic metabolic disorder characterized by hyperglycemia resulting from insulin secretion defects or insulin resistance(IR).[1] The primary types include type 1 diabetes (T1DM), type 2 diabetes (T2DM), and gestational diabetes mellitus (GDM).[2] T2DM is characterized by a reduction in insulin production or IR, leading to elevated blood glucose levels.[3] According to the latest data from the International Diabetes Federation (IDF), the global prevalence of T2DM among adults was estimated to be 536.6 million (10.5%) in 2021, with projections indicating a further increase to 783.2 million (12.2%) by 2045.[4,5] There is substantial evidence demonstrating that a significant proportion of T2DM cases can be prevented through the adoption of healthy lifestyle behaviors, including maintaining a normal body weight, following a nutritionally balanced diet, engaging in regular moderate to vigorous physical activity, abstaining from tobacco use, and consuming alcohol in moderation, both within the general population and among individuals at increased risk,[6,7] such as those with elevated fasting plasma glucose levels.[8]

Western medicine's diagnosis, treatment, and medication often fall short of achieving satisfactory therapeutic effects and tolerability, making it challenging to meet individual treatment needs. Traditional Chinese medicine (TCM).[9] Dangguiliuhuang Tang (DGLHT) is a classic TCM formula commonly used to treat T2DM. Originating from Li Dongyuan's "LanTingMiCang" during the Jin and Yuan dynasties (1180–1251 AD), this formula comprises seven herbs: Angelicae Sinensis Radix, Rehmanniae Radix, Rehmanniae Radix Praeparata, Scutellariae Radix, Coptidis Rhizoma, Phellodendri Chinese Cortex, and Astragali Radix, in a ratio of 1:1:1:1:1:1:2. The National Administration of Traditional Chinese Medicine has now included it in the *First Batch of Ancient Classical Prescriptions Catalog*. Key

components include ferulic acid, catalpol, and berberine. Previous research demonstrated DGLHT's effectiveness in treating T2DM by regulating the interaction between dendritic cells and T lymphocytes, although its precise mechanism and material basis remain unclear. DGLHT's unique combination of *Radix Rehmanniae* and *Rehmanniae Radix Praeparata* has been shown to enhance the expression levels of inflammation and energy metabolism-related proteins in the liver of T2DM mice.[10] Our team's previous research and current research demonstrated that these herbs ameliorate inflammation, oxidative stress, and autophagy dysfunction in T2DM mice.[11,12] As a classic traditional Chinese medicine formula, DGLHT has been increasingly used as an adjunctive therapy for DM in recent years, with multiple clinical studies reporting its potential efficacy. However, the precise mechanisms underlying its hypoglycemic effects, particularly its influence on the composition and function of the gut microbiota, have not been systematically elucidated. Furthermore, the key active constituents responsible for its pharmacological actions, as well as their in vivo metabolic processes, remain poorly characterized, resulting in an insufficient understanding of its material basis. These limitations hinder the modern application and in-depth development of DGLHT. Therefore, further investigation into the mechanisms by which DGLHT modulates the gut microbiome and clarification of its pharmacodynamic material basis are crucial to unveil the scientific rationale behind its anti-diabetic effects.

Each individual technology is limited in its ability to capture the full biological complexity of most human diseases. As a result, the integration of multiple technologies has emerged as a promising approach to provide a more comprehensive understanding of biological systems and disease mechanisms.[13] This study employs a multi-omics collaborative research approach to investigate the material basis and mechanisms of action of DGLHT in treating T2DM. Ultra-high-performance liquid chromatography coupled with Thermo Vanquish UHPLC-Thermo Q Exactive HFX (UHPLC-QE-MS) was utilized to identify the chemical components of DGLHT. A potential therapeutic network for DGLHT in treating T2DM was constructed using network pharmacology. Untargeted metabolomics techniques were applied to reveal the differential effects of DGLHT on T2DM, and 16S rDNA amplification sequencing technology was used to investigate the differential metabolic regulation of gut microbiota in T2DM mice treated with DGLHT. Molecular biomedical experimental methods were combined to validate and analyze relevant molecular pathways in the liver. A correlation analysis between the active ingredients of DGLHT and the differential gut microbiota was established. In summary, this study provides a preliminary clarification of the material basis of DGLHT and elucidates its effects and mechanisms in treating T2DM, contributing valuable insights to the field of traditional Chinese medicine, particularly in the prevention and treatment of T2DM.

Materials and Methods

Reagents and Materials

Angelicae Sinensis Rdixa, Radix Rehmanniae, Rehmanniae Radix Praeparata, Scutellariae Radix, Coptidis Rhizoma, Phellodendri Chinese Cortex, and Astragali Radix were purchased from Shanxi Herentang Traditional Chinese Medicine Yinpian and Ltd. Co. (Lot No.:220805, 220302, 220401, 191108, 220501, 220403, 220504, Taiyuan, Shanxi, China) and were evaluated by Professor Shuosheng Zhang (Shanxi University of Chinese Medicine) before use. Angelicae Sinensis Rdixa is the dried root of *Angelica sinensis* (Oliv.) Diels, a plant in the Umbelliferae family. Radix Rehmanniae is the dried root of *Rehmanmia glutinosa* Libosch., a plant in the Scrophulariaceae family. *Rehmanniae Radix Praeparata* is a processed product of Radix Rehmanniae. *Scutellariae Radix* is the dried root of *Scutellaria baicalensis* Georgi, a plant in the Lamiaceae family. *Coptidis Rhizoma* is the dried rhizome of *Coptis chinensis* Franch., a plant in the Ranunculaceae family. *Phellodendri Chinese Cortex* is the dried bark of *Phellodendron chinense* Schneid., a plant in the Rutaceae family. Astragali Radix is the dried root of *Astragalus membranaceus (Fisch.)* Bge.var.mongholicus (Bge.) Hsiao, a leguminous plant. Voucher specimens (No. SXTCM-Meng-2023111 for Angelicae Sinensis Rdixa, SXTCM-Meng -2023112 for Radix Rehmanniae, SXTCM-Meng-2023113 for Rehmanniae Radix Praeparata, SXTCM-Meng-2023114 for Scutellariae Radix, SXTCM-Meng-2023115 for Coptidis Rhizoma, SXTCM-Meng-2023116 for Phellodendri Chinese Cortex, SXTCM-Meng-2023117 for Astragali Radix) were deposited in the Herbarium of Shanxi University of Chinese Medicine (SXTCM), Jinzhong, China.

Streptozotocin (STZ, Lot No.: WXBC6558V, Sigma, USA) was used in conjunction with a Sanno blood glucose meter and test strip (Lot No.: 2J01E210813, Sanno Biosensing Co., Ltd., Changsha, China). The following antibodies were employed: phosphorylated phosphatidylinositol 3-kinase/phosphatidylinositol 3-kinase (p-PI3K/PI3K), phosphorylated protein kinase/protein kinase (p-AKT/AKT), phosphorylated AMP-dependent protein kinase/AMPK (p-AMPK/AMPK), silent information regulator sirtuin 1(Sirt1), peroxisome proliferator-activated receptor gamma coactivator alpha Or 1 alpha (PGC-1 alpha), β-actin, glucose transporter type 4 (GLUT4), phosphorylated nuclear factor kappa-B/nuclear factor kappa-B (p-NF-κB/NF-κB), Toll-like receptor 4 (TLR4) (Lot No.: AP0854/A4992, AP0432/A12718, AP0124/A19653, A18675, A11267, AC026, A12348, AC038/A7637, A5258, ABclonal Co., Ltd., Wuhan, China); HRP sheep anti-rabbit IgG, Catalase(CAT), Heme Oxygenase-1(HO-1), NOD-like receptor thermal domain-associated protein 3 (NLRP3), superoxide dismutase 2 (SOD2) (Lot No.:BA1039, BA0605, PB0971, BST18G21CA18I54, AAD23161, BOSTER Biological Technology Co., Ltd., Wuhan, China). Additionally, an SDS-PAGE gel preparation kit, enhanced RIPA lysate (Lot No.: CR2202061, 18C23C02, BOSTER Biological Technology Co., Ltd., Wuhan, China), TBST solution (batch number: 20240703, Solaibao Technology Co., Ltd., Beijing, China), phosphate buffer solution (PBS, Lot No.: GA23090231725, Servicebio Technology Co., Ltd., Wuhan, China), and protein molecular weight standards (BeyoColorTM Color Pre-Stained Protein Molecular Weight Standards [19–117kD, 15–120kD, 10–150kD, 14.4–116kD] and M5 Precise Prestige Protein Ladder [15–120 kDa, 15–136kD]) were utilized (Lot No.: P0066 P0078, P0060s, P0062, Beyotime Biotechnology Co., Ltd., Shanghai, China; Lot No.: 24GH0423, 24GH0517, Mei5 Biotechnology Co., Ltd., Beijing, China).

The GeneGnome system (GeneGnome XRQ, Gene, USA), ImageJ (ImageJ 2, NIH, USA), and GraphPad Prism (version 5.0; GraphPad Software, La Jolla, CA, USA) were used for data analysis. For UHPLC-MS analysis, a Thermo UHPLC Vanquish system coupled with a Q Exactive HF-X Hybrid Quadrupole Orbitrap Mass Spectrometer (Thermo Fisher Technology Co., LTD, CA, US) was employed. An ACQUITY UpLC HSS T3 column (2.1 mm × 100 mm, 1.8 μm) (Waters Co., LTD, MA, US) was used for chromatographic separation.

Experimental Methods

Grouping and Treatment of Experimental

Male C57BL/6 mice (SPF grade, 7 weeks old, body weight 18–22 g) were obtained from SPF Biotechnology Co., Ltd., Beijing, China (Animal license number: SCXK (Jing) 2019-0010). The mice were housed under standard conditions with a temperature of (23 ± 2) °C, relative humidity of (50 ± 10)%, and a 12-hour light/12-hour dark cycle. The mice had free access to food and water. All mice were acclimated for one week before the experiment. The experiment was approved by the Ethics Committee of Shanxi University of Traditional Chinese Medicine (Approval No. 2022DW087) and conducted in accordance with national guidelines (Laboratory animal—Guideline for ethical review of animal welfare, GB/T 35892-2018). In our experiments, we followed the blinded design protocols outlined in the ARRIVE guidelines 2.0 to minimize experimental bias.

Preparation of DGLHT

Angelicae Sinensis Radix, Radix Rehmanniae, Rehmanniae Radix Praeparata, Scutellariae Radix, Coptidis Rhizoma, Phellodendri Chinensis Cortex, and Astragali Radix were combined in a ratio of 1:1:1:1:1:1:2 and soaked in twice their volume of distilled water for 30 minutes. Subsequently, eight times the volume of distilled water was added, and the mixture was heated and refluxed for 40 minutes. The solution was then filtered, and the remaining residue was treated with six times its volume of distilled water and heated and refluxed for an additional 40 minutes. The two extracts were combined and concentrated under reduced pressure to obtain a water decoction with a concentration of 0.13 g/mL.

Preparation and Administration of the T2DM Mice Model

After a one-week acclimatization period, 6 mice were randomly selected to serve as the normal control group, while the remaining 24 mice were intraperitoneally injected with 100 mg/kg of STZ for modeling (once daily for 3 consecutive days). Fasting blood glucose (FBG) levels were measured on the 3rd, 7th, and 14th days following the injection. An FBG level ≥ 11.1 mmol/L after stabilization indicated successful modeling. The successfully modeled mice were then

randomly divided into four groups: a model group (Model), a low-dose group of Danggui Liuhuang Tang (Low Dose, 1.95 g/kg), a high-dose group of Danggui Liuhuang Tang (High Dose, 3.9 g/kg), and a metformin group (Metformin, 250 mg/kg),[11] with 6 mice in each group. Dosages were adjusted according to the clinical daily dose for a 70 kg adult human. The mice in the Control and Model groups were orally administered the same volume of purified water for 4 consecutive weeks.

On the 25th day of administration, after a 12-hour fasting period, an oral glucose tolerance test (OGTT) was conducted by gavaging a glucose solution (2 g/kg). Blood was collected through the tail vein at 0, 15, 30, 45, 60, 90, and 120 minutes to measure blood glucose levels. The changes in blood glucose levels over time were recorded, and the area under the curve (AUC) was calculated using the linear trapezoidal method. After 4 weeks of administration, an insulin tolerance test (ITT) was conducted. The mice were fasted for 3 hours, and their fasting blood glucose levels were measured. Insulin (0.5 U/kg) was injected intraperitoneally, and blood glucose levels were measured at 15, 30, 45, and 60 minutes, with the AUC for each group calculated. One day before the conclusion of the experiment, a second sample of fresh feces from mice subjected to tail-lifting stress defecation was collected from a sterile operating table and quickly transferred to a sterile freezing tube for storage at −80°C. Following the final administration, the mice were fasted without water for 12 hours. After anesthesia with 2% isoflurane, blood was collected from the abdominal aorta, centrifuged (4000 rpm/min, 15 minutes, 4°C), and serum was collected and stored at −80°C for future use. The mouse liver was then fixed in 4% formaldehyde or stored at −80°C for further analysis.

Hematoxylin and Eosin (H&E) Staining

After collecting blood from the mice, liver samples were obtained and fixed in 4% paraformaldehyde for 72 hours. The samples were subsequently decalcified, washed, dehydrated with ethanol, cleared, and embedded in paraffin. The resulting sections were then examined and photographed using a microscope.

UHPLC-QE-MS

Metabolite extraction: After thawing the samples at 4°C, an appropriate amount was aliquoted and mixed with pre-cooled methanol/acetonitrile/water solution (2:2:1, v/v/v). The mixture was vortexed and subjected to low-temperature ultrasonication for 30 minutes, followed by incubation at −20°C for 10 minutes. Subsequently, the samples were centrifuged at 14,000 g and 4°C for 20 minutes. The supernatant was collected and vacuum-dried. For mass spectrometry analysis, the dried extract was reconstituted in 100 μL of acetonitrile/water solution (acetonitrile: water= 1:1, v/v), vortexed, and centrifuged again at 14,000 g and 4°C for 15 minutes. The final supernatant was used for injection and analysis.

Chromatographic conditions for serum metabolites: ACQUITY UPLC HSS T3 chromatographic column. The mobile phase consisted of a 0.1% formic acid aqueous solution (A) and a 0.1% formic acid acetonitrile solution (B). Gradient elution was employed as follows: from 0.0 to 17.0 minutes, the composition was 95% A and 5% B; from 17.0 to 17.2 minutes, the composition shifted to 2% A and 98% B; and from 17.2 to 20.0 minutes, the composition returned to 95% A and 5% B. The flow rate was set at 0.3 mL/min, and the column temperature was maintained at 35°C. Mass spectrometry parameters: Q-Exactive HFX mass spectrometer, utilizing both positive and negative ion acquisition modes. Test conditions: spray voltage was −3500V and 3800V, respectively; the sheath gas pressure was maintained at 45 arbitrary units,[14] while the auxiliary gas pressure was set to 20 arb. The ion transport tube temperature was 320°C, and the atomization temperature was 350°C. The scanning range was from 90 to 1300 m/z.

Chromatographic conditions were established using an Agilent 1290 Infinity LC HILIC chromatographic column. The mobile phase consisted of a 0.1% formic acid aqueous solution (A) and a 0.1% formic acid acetonitrile solution (B). A gradient elution was employed, starting with 95% B (0–0.5 minutes), followed by a linear decrease to 65% B (0.5–7.0 minutes), then to 40% B (7.0–8.0 minutes), maintaining 40% B for 1.0 minutes (8.0–9.0 minutes), and finally increasing to 95% B (9.0–9.1 minutes), which was held for the remaining 2.9 minutes (9.1–12.0 minutes). The flow rate was maintained at 0.5 mL/min, and the column temperature was kept constant at 25°C.

Mass spectrometry parameters were optimized for the AB Triple TOF 6600 Mass Spectrometer, operating in both positive and negative ion acquisition modes. Test conditions included a spray voltage of −5500 V for negative ion mode

and 5500 V for positive ion mode, a sheath pressure of 45 arbitrary units (au), an auxiliary gas pressure of 20 au, a transmission capillary temperature of 320°C, a probe heater temperature of 370°C, and a scanning range of 90–1300 m/z.

The UPLC-QE-MS method was employed to identify the chemical components in mice serum both before and after administration. Secondary Spectrum (MS2) data was compared with the mass spectrometry database. Screening criteria were established based on MS2 fragment similarity scores exceeding 0.7, allowing for the identification of components with higher concentrations. Differential components were imported into the MetaboAnalyst platform for pathway enrichment analysis, using criteria of an impact value greater than 0.1 and a *P*-value less than 0.05.

Chromatographic conditions for rehmannioside D and ferulic acid were as follows: a HypersilGOLD DaQC18 column (4.6 mm × 250 mm, 5 μm) was used with a flow rate of 1.0 mL/min and an injection volume of 10 μL. The column temperature was maintained at 25°C. To determine the ferulic acid content, the mobile phase consisted of acetonitrile and 0.1% phosphoric acid aqueous solution (17:83), employing isocratic elution with a detection wavelength of 322 nm. To determine the content of rehmannioside D, the mobile phase was composed of acetonitrile and 0.1% phosphoric acid aqueous solution (30:70), employing isocratic elution with a detection wavelength of 203 nm. A standard solution of ferulic acid was prepared with a mass concentration of 510.5 μg/mL, and a standard solution of rehmannioside D was prepared with a mass concentration of 501.4 μg/mL. Methanol served as a blank control. A DGLHT solution with a mass concentration of 0.05 g/mL was filtered through a 0.45 μm microporous membrane to obtain the test solution, and three parallel samples were prepared. High-performance liquid chromatography (HPLC) was utilized to detect the content of ferulic acid and rehmannioside D in the DGLHT.

Information was gathered from Chemicalbook (https://www.chemicalbook.com/), Chemspider (https://chemspider.com), PubMed (https://pubmed.ncbi.nlm.nih.gov), and Scifinder (https://scifinder.cas.org). A database was then established that included the molecular formula, molecular weight, chemical name, and chemical structure of relevant compounds. UHPLC-QE-MS analysis was subsequently performed on the serum of DGLHT-treated mice and mice with T2DM. This analysis was conducted according to previously established liquid chromatography and mass spectrometry conditions.

Network Pharmacology Analysis

Following the analysis of DGLHT as described in UPLC-QE-MS Section, relevant target keywords, including Angelicae Sinensis Radix, Radix Rehmanniae, Rehmanniae Radix Praeparata, Scutellariae Radix, Coptidis Rhizoma, Phellodendri Chinensis Cortex, and Astragali Radix were investigated in the context of T2DM. This investigation utilized the Traditional Chinese Medicine Systems Pharmacology Database and Analysis Platform (TCMSP) (https://old.tcmsp-e.com/tcmsp.php), the Traditional Chinese Medicine Integrative Database (TCMID) (http://www.megabionet.org/tcmid/), and the Comparative Toxicology Database (CTD) (http://ctdbase.com/). Subsequently, Uniprot (https://www.uniprot.org/) was employed to standardize gene names across the databases. To identify potential active ingredients in traditional Chinese medicine for diabetes treatment, a comparison was conducted between the potential action targets of identified compounds and known disease targets. String database (https://cn.string-db.org/) was then used to analyze key targets and their protein interactions. Network topology analysis and generation of relevant network diagrams were performed using NetworkX (networkx-2.8.2, https://networkx.org). Furthermore, Gene Ontology (GO) database (https://geneontology.org) and Kyoto Encyclopedia of Genes and Genomes (KEGG) database (https://www.kegg.jp/) were utilized for GO and KEGG analysis, respectively. Finally, the results of this pathway enrichment analysis were visualized using the R programming language.

Gut Microbiota

Extraction of genome DNA: Total genome DNA from samples were extracted using Mag-bind soil DNA kit (Omega). DNA concentration and purity were monitored on 1% agarosegels. According to the concentration. Amplicon Generation: 16S rRNA genes were amplified used the specific primer with the barcode. All PCR reactions were carried out in 30 μL reactions with 15 μL of Phusion High-Fidelity PCR Master Mix (New England Biolabs); 0.2μM of forward and reverse primers, and about 10 ng template DNA. Thermal cycling consisted of initial denaturation at 98 °C for 1 min,

followed by 30 cycles of denaturation at 98°C for 10s, annealing at 50 °C for 30s, and elongation at 72 °C for 30s. Finally 72 °C for 5 min. PCR Products quantification and qualification: Mix same volume of 1X loading buffer (contained SYB green) with PCR products and operate electrophoresis on 2% agarose gel fordetection. Samples with bright main strip between 400–450 bp were chosen for further experiments.

Intestinal samples from mice were collected, followed by DNA extraction and amplification via PCR. The V3-V4 regions of 16S rRNA genes were subsequently sequenced using the Illumina NovaSeq 6000.[15] Abundance level curves were drawn based on the operational taxonomic unit (OTU) abundance distribution for each sample. Additionally, alpha diversity indices, including Observed Species, Shannon, Simpson, Chao 1, ACE, Coverage, and PD whole tree, were calculated to assess the diversity of gut microbiota components.

In this experiment, the following measures were implemented to control contamination: Negative Controls: Extraction negative controls were included in each DNA extraction procedure, and amplification negative controls were included in each PCR amplification. All negative controls were subjected to subsequent sequencing analysis alongside the samples. Standardized Operating Procedures (SOPs): A unified and standardized protocol was strictly followed for sample collection, storage, DNA extraction, and PCR amplification. All procedures were conducted within dedicated laminar flow hoods or PCR workstations. Operators wore gloves, masks, and caps; work surfaces were regularly decontaminated; and UV sterilization was routinely applied. Reagent Batch Control: Wherever possible, all samples were processed using the same batch of DNA extraction kits, PCR reagents, and sequencing kits.

Western Blotting

Protein was extracted from mouse liver using cell lysate and its content measured via the BCA method. Subsequently, the protein was isolated using Sodium Dodecyl Sulfate Polyacrylamide Gel Electrophoresis (SDS-PAGE) and transferred to NC membrane. The membrane was blocked with 5% skim milk at room temperature for 2 hours, followed by incubation with antibodies against p-NF-κB (p65)/NF-κB (p65), TLR4, NLRP3, p-PI3K/PI3K, p-AKT/AKT, GLUT4, HO-1, SOD2, CAT, p-AMPK/AMPK, Sirt1, and PGC-1α at 4°C overnight. After washing the membrane three times with TBST, it was incubated with HRP-conjugated sheep anti-rabbit IgG at room temperature for 4 hours. Finally, the membrane was exposed using the GeneGnome imaging system, and the relative expression levels of the proteins were analyzed using ImageJ software.

Data Analysis

Statistical analyses on various experimental datasets were performed using GraphPad Prism 8.0 software, and the resulting plots were generated. The data was subjected to the Shapiro–Wilk normality test. Data that conformed to a normal distribution were expressed as mean ± SD. One-way analysis of variance (ANOVA) was used to compare differences between sample groups, and Tukey's post-hoc test was conducted for pairwise comparisons between groups. A *P*-value of less than 0.05 was considered statistically significant.

Gut microbiota statistical analyses were performed on the preprocessed community data, encompassing T-tests, Wilcoxon rank sum tests, and Tukey's tests to evaluate intergroup differences in beta diversity based on weighted Unifrac and unweighted UnifracBeta distances. For each sample or group, the top 10 species with the highest abundance rankings at each taxonomic classification level (Phylum, Class, Order, Family, Genus, Species) were identified and visualized in a bar chart representing their relative abundance and proportions across different classification levels. STAMP differential analysis was employed to compare species abundance among multiple sample groups (Kruskal Wallis test analysis) and identify significantly different species, a *P*-value of less than 0.05 was considered statistically significant. Furthermore, Phylogenetic Investigation of Communities by Reconstruction of Unobserved States (PICRUSt) software was used to predict the metabolic functions of microbial communities based on the species composition information derived from the 16S sequencing data. A relative abundance bar graph was created to illustrate the abundance distribution of each functional group within the sample group.

Correlation analysis: Spearman's statistical method was used to analyze the correlation coefficients between the components and differential components of the DGLHT compound identified in UHPLC-QE-MS Section, as well as the differential microbiota obtained in Gut microbiota Section. This analysis was conducted using R 3.4.2 language software

to explore the potential interactions between the microbiota and the components of DGLHT. Microbiome data and TCM constituent data frequently violate the assumption of normal distribution and often contain zero values or extreme values.

Results

DGLHT Alleviates Abnormal Blood Glucose Levels and Glucose Tolerance in Mice with T2DM

Compared to the Control group, the FBG levels of mice in the Model group were significantly elevated ($P < 0.0001$ in weeks 1–4). Conversely, the FBG levels of mice in the low dose group ($P < 0.0001$ in weeks 1–3), high-dose group ($P < 0.0001$ in weeks 1–2 and $P < 0.001$ in week 3), and Metformin group ($P < 0.0001$ in weeks 1–2 and $P < 0.001$ in week 3) were significantly reduced compared to the Model group. These experimental results demonstrate that DGLHT can effectively lower FBG levels in T2DM mice (Figure 1A).

In the OGTT experiment, Model group mice exhibited a significant increase in average blood glucose levels compared to the Control group at various time points: 0 minutes ($P < 0.05$), 30 minutes ($P < 0.01$), 45 minutes ($P < 0.0001$), 60 minutes ($P < 0.001$), 90 minutes ($P < 0.0001$), and 120 minutes ($P < 0.001$) following glucose injection. Conversely, mice in each treatment group demonstrated a significant decrease in blood glucose levels at 15, 30, 45, 60, 90, and 120 minutes post-glucose injection compared to the Control group. Additionally, the area under the curve (AUC) for the Model group was significantly higher than that of the Control group ($P < 0.0001$). Furthermore, the AUC for the low-dose group ($P < 0.0001$), high-dose group ($P < 0.0001$), and Metformin group ($P < 0.0001$) was significantly reduced compared to the Model group (Figure 1B). These experimental results collectively suggest that DGLHT can effectively enhance glucose tolerance in T2DM mice.

In the ITT experiment, blood glucose levels in the Model group of mice significantly decreased after 15 minutes of insulin injection compared to the Control group ($P < 0.05$). Both the high-dose group ($P < 0.05$) and the Metformin group ($P < 0.05$) also exhibited a significant reduction in average blood glucose levels following 15 minutes of intraperitoneal insulin injection. However, blood glucose levels in the Metformin group demonstrated a significant increase after 45 minutes ($P < 0.05$) and 60 minutes ($P < 0.05$) of insulin injection. The AUC for the Model group was higher compared to the Control group. In contrast, the AUC for the low-dose group ($P < 0.0001$) and the high-dose group ($P < 0.001$) was significantly lower than that of the Model group (Figure 1C). These experimental results suggest that DGLHT can effectively alleviate IR in T2DM mice.

DGLHT Alleviates Liver Injury in T2DM Mice

H&E staining revealed that the Control mice exhibited a normal liver lobule structure with neatly arranged hepatic cords and radially organized liver cells devoid of fat vacuoles. In contrast, the Model group displayed a disrupted liver lobule structure, characterized by disordered hepatic cords and unevenly sized fat vacuoles within the liver cells. Compared to the Model group, the Metformin, low-dose, and high-dose groups demonstrated well-defined liver lobule structures with neatly arranged hepatic cords and radially organized liver cells. Notably, the high-dose and Metformin groups exhibited a significant reduction in intracellular fat vacuoles (Figure 1D), suggesting that DHLHT can effectively ameliorate liver damage in T2DM mice.

DGLHT Component Identification

To obtain comprehensive data, the experiment utilized both positive and negative ion modes of electrospray ionization for mass spectrometry analysis. By comparing the results with the mass spectrometry database, a total of 3051 chemical components were identified within the DGLHT compound and its individual drug samples. The peak shapes of chromatographic peaks with high abundance were confirmed. In the positive ion mode, the following compounds were identified: L-tryptophan, Magnoflorine, Epiberberine, Berbericinine, Apigenin 7-glucuronide, Naringenin, Genistin-4′-glucuronide, baicalin, Chrysoeriol, and 7,8,3′-trihydroxyflavone. In the negative ion mode, 17 chemical components were identified, including Cynarin, Heriguard, Apigenin 7-glucuronide, Baicalin, Oroxyloside, Baicalein, and Neobaicalein. Additionally, 21 chemical components were identified in both ion modes, including 3′-trihydroxyflavone, Neobaicalein II, Comanthoside B, Ferulic acid, and Rehmanniaside D (Figure 2A). The concentrations of Ferulic acid and Rehmanniaside D were 1.18 ± 0.37 μg/mL and 198.39 ± 19.89 μg/mL, respectively.

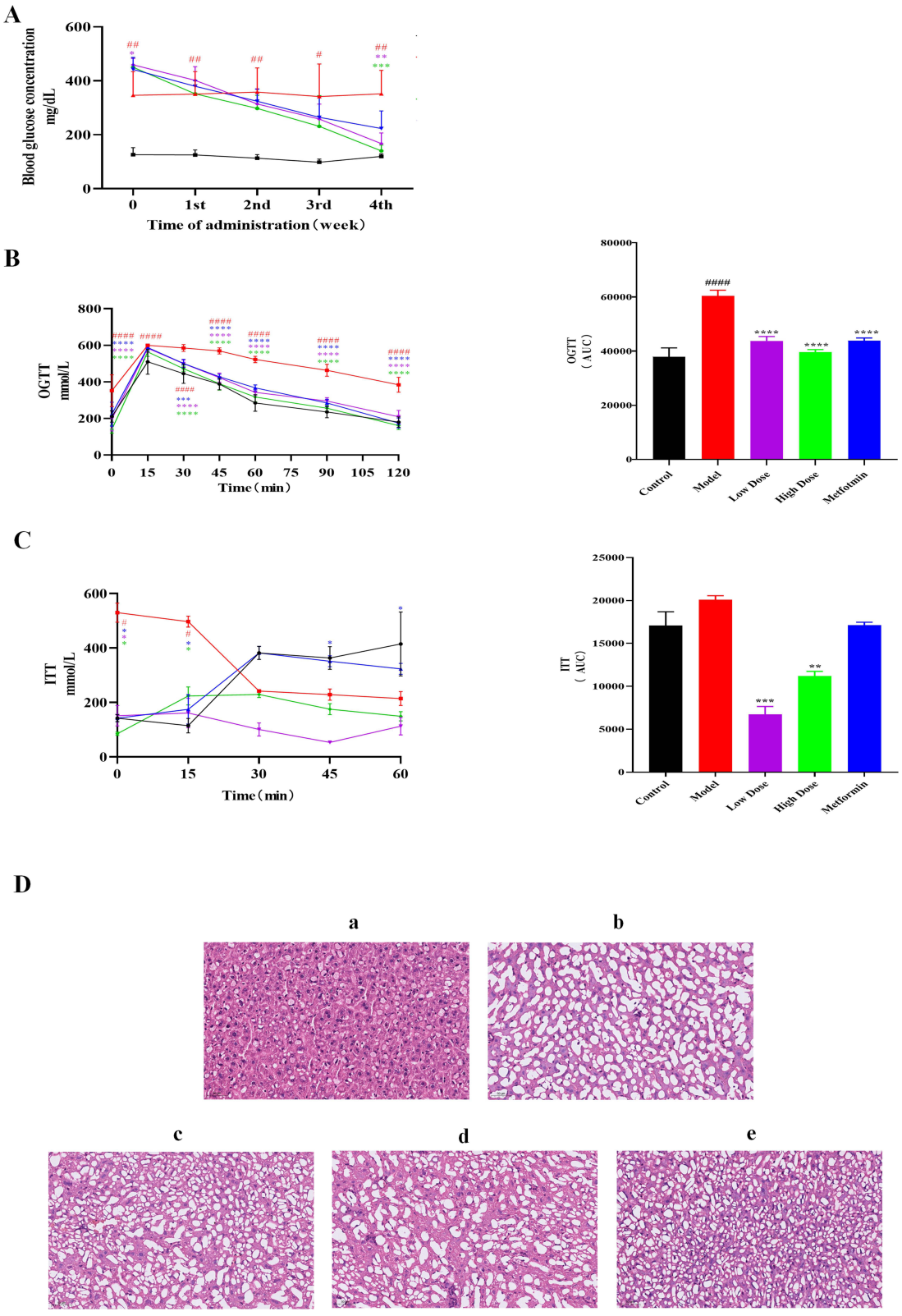

Figure 1 Effects of DGLHT on blood glucose levels, glucose tolerance, and liver in T2DM mice. (**A**) The effect of DGLHT on fasting blood glucose levels in T2DM mice. (**B**) The effect of DGLHT on glucose tolerance in T2DM mice. (**C**) The effect of DGLHT on insulin resistance in T2DM mice. (**D**) HE staining of liver tissues in DMD mice (All images were tak under a 40x microscope). (a) Control group; (b) Model group; (c) Low dose group; (d) High dose group; (e) Metformin group. Six samples were analyzed for each group. Data are presented as mean ± SD. The data were analyzed using an unpaired *t*-test. $^{\#}P<0.05$, $^{\#\#}P<0.01$, $^{\#\#\#\#}P<0.0001$ vs Control group, $^{*}P<0.05$, $^{**}P<0.01$, $^{***}P<0.001$, $^{****}P<0.0001$ vs Model group.Bar graphs show mean ± SD. Black indicates the control group, red indicates the model group, purple indicates the low dose group, green indicates the high dose group and blue indicates the metformin group.

https://doi.org/10.2147/DMSO.S525913

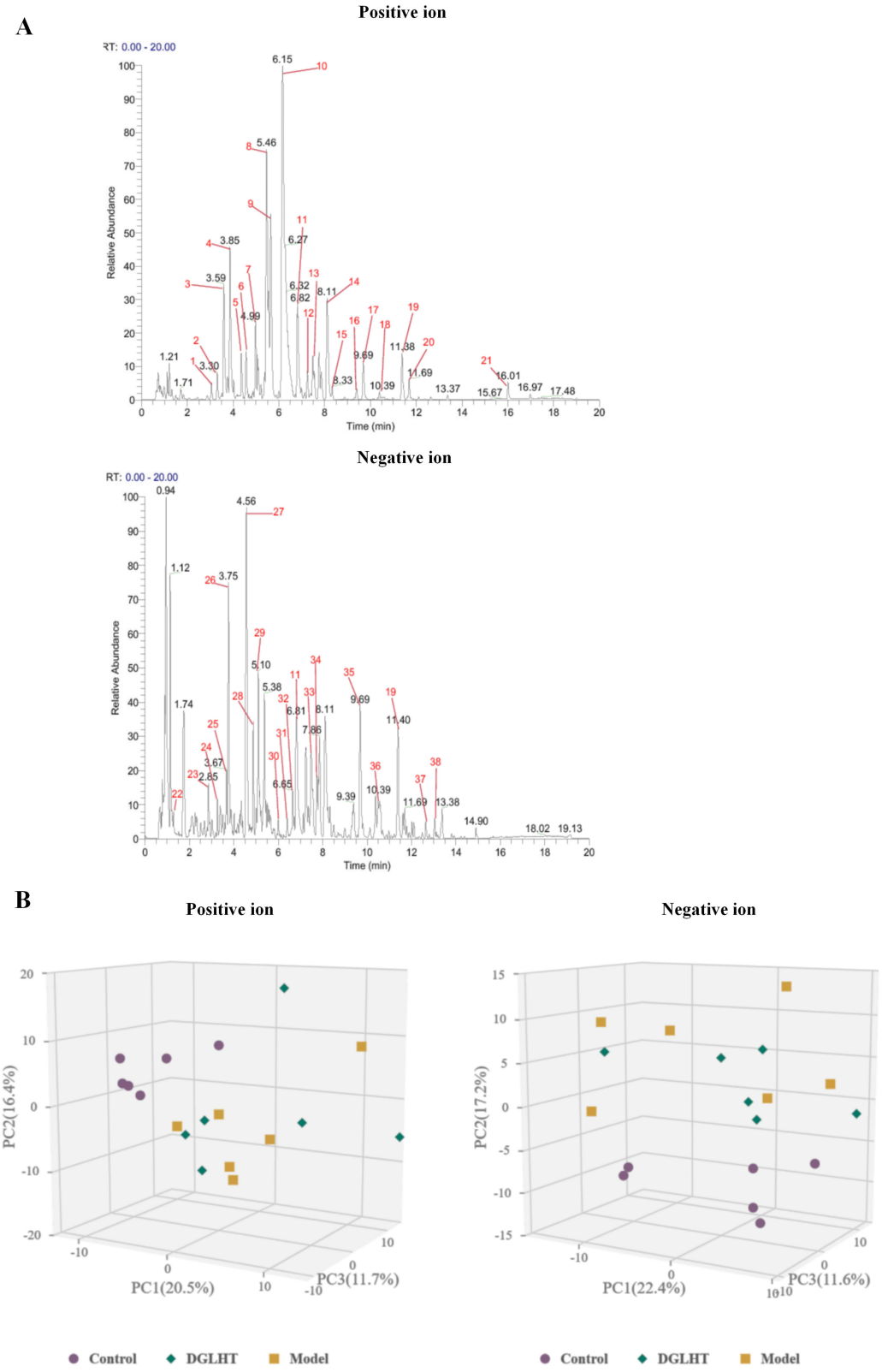

Figure 2 Component identification of DGLHT and its effect on metabolites in T2DM mice. (**A**) Under positive and negative ion modes, the abundance of DGLHT reaches its peak. 1–21: High-abundance peaks in positive ion mode. 22–38: High-abundance peaks in negative ion mode. (**B**) Under positive and negative ion modes, PCA analysis of differential metabolites in the liver of T2DM mice. Six samples were analyzed for each group.

Untargeted Metabolomics

A total of 1941 components were identified in the Control, Model, and DGLHT groups. Principal component analysis (PCA) was performed on liver components in both positive and negative ion modes to highlight differences among the groups. The PCA score plot revealed that the cumulative variance for positive and negative ion modes was 48.1% and 51.2%, respectively, capturing most of the metabolic variation. In both ion modes, a clear separation trend was observed among the Control, Model, and DGLHT groups. Following DGLHT intervention, components levels returned to those of the Control group (Figure 2B). A comparison of the Total Ion Chromatogram[16] of Quality Control (QC) samples, which displayed overlapping spectra, demonstrated minimal experimental error and reliable data quality.

The Orthogonal Partial Least Squares Discriminant Analysis (OPLS-DA) results (statistical thresholds are VIP>1, $P<0.05$) demonstrated a clear separation of metabolic profiles between the Control group and the Model group, as well as between the Model group and the DGLHT group, suggesting that this model is suitable for screening differential components (Figure 3A). The OPLS-DA model was validated through permutation testing, which revealed that all simulated values were lower than the true values (VIP>1.0), and the Q2 regression line intercepts were below −0.05. These findings indicated a good model fit, predictive ability, and the absence of overfitting (Figure 3B).

According to the OPLS-DA results, compounds with VIP values greater than 3 and P values less than 0.05 were identified as potential differential components for DGLHT treatment of T2DM through FC plot analysis. Ultimately, the Control group and Model group exhibited 119 differential components, including 56 upregulated differential components such as phenylpropanoids, lipids, and organic acids (eg, 2,6-di-tert-butylphenol, Erucic acid, Betaine, Glutathione) and 63 downregulated differential components such as alkaloids, organic heterocycles, phenylpropanoids, and polyketides (eg Trigonelline, 4-hydroxyquinoline, Daidzein 4′-sulfate, hydroxyphenylacetic acid). In comparing the Model and DGLHT groups, 31 differentially expressed components were identified, with 17 upregulated and 14 downregulated. Table 1 provides a list of some significant components. Notably, after DGLHT intervention, 8 components were downregulated compared to the Model group, including 5-hydroxyindole, D-galactouronic acid, glycocholic acid, prostaglandin F2α, succinic acid, 9-cis-retinal, isopimaric acid, and methionine sulfide. The KEGG pathway enrichment results indicated that the most significant differences in metabolic pathways between the Model group and both the low-dose and high-dose groups were bile secretion, cholesterol metabolism, biosynthesis of unsaturated fatty acids, protein digestion and absorption, cysteine and methionine metabolism, and primary bile acid biosynthesis (Figure 3C).

Establishment of a Treatment Network for T2DM with Active Ingredients of DGLHT

After screening and deduplication, 693 potential DGLHT targets were identified, and 19,751 diabetes-related genes were sourced from the CTD database. The intersection of these two sets yielded 693 potential targets for DGLHT treatment of T2DM (Figure 4A). Using the KEGG platform, pathway function annotation and enrichment analysis were conducted on the core targets. Results indicated that 50 core targets were linked to 107 KEGG pathways (Figure 4B and C). Analyzing the top 20 pathways based on P value ($P < 0.05$), key pathways identified for DGLHT treatment of T2DM included the cancer signaling, MAPK, and ErbB pathways. A key component core target pathway network was then constructed from these top 20 results, which included Wortmannin, Gallic acid, Morphine, and Isoquercin. This network comprised 48 core targets, including mitogen-activated protein kinase 1 (MAPK1), mitogen-activated protein kinase 3 (MAPK3), serine/threonine kinase 1 (AKT1), tyrosine kinase non-receptor (TNK), and C-X-C motif chemokine ligand 8 (CXCL8), which may be key targets. Additionally, 20 related pathways, such as Cell cycle, Neurotrophin signaling pathway, Chemokine signaling pathway, ErbB signaling pathway, and Toll-like receptor signaling pathway, were identified (Figure 4D).

Gut Microbiota

The richness of intestinal bacteria was assessed using various alpha diversity indices. Compared to the Control group, mice in the Model group exhibited higher Observed Species, Shannon, Simpson, Chao 1, and ACE indices but lower Coverage and Phylogenetic Diversity(PD) whole tree indices. In the DGLHT group, these trends were partially reversed, with decreases in Observed Species, Shannon, Simpson, Chao 1, and ACE indices, and increases in Coverage and PD whole tree indices (Figure 5A).

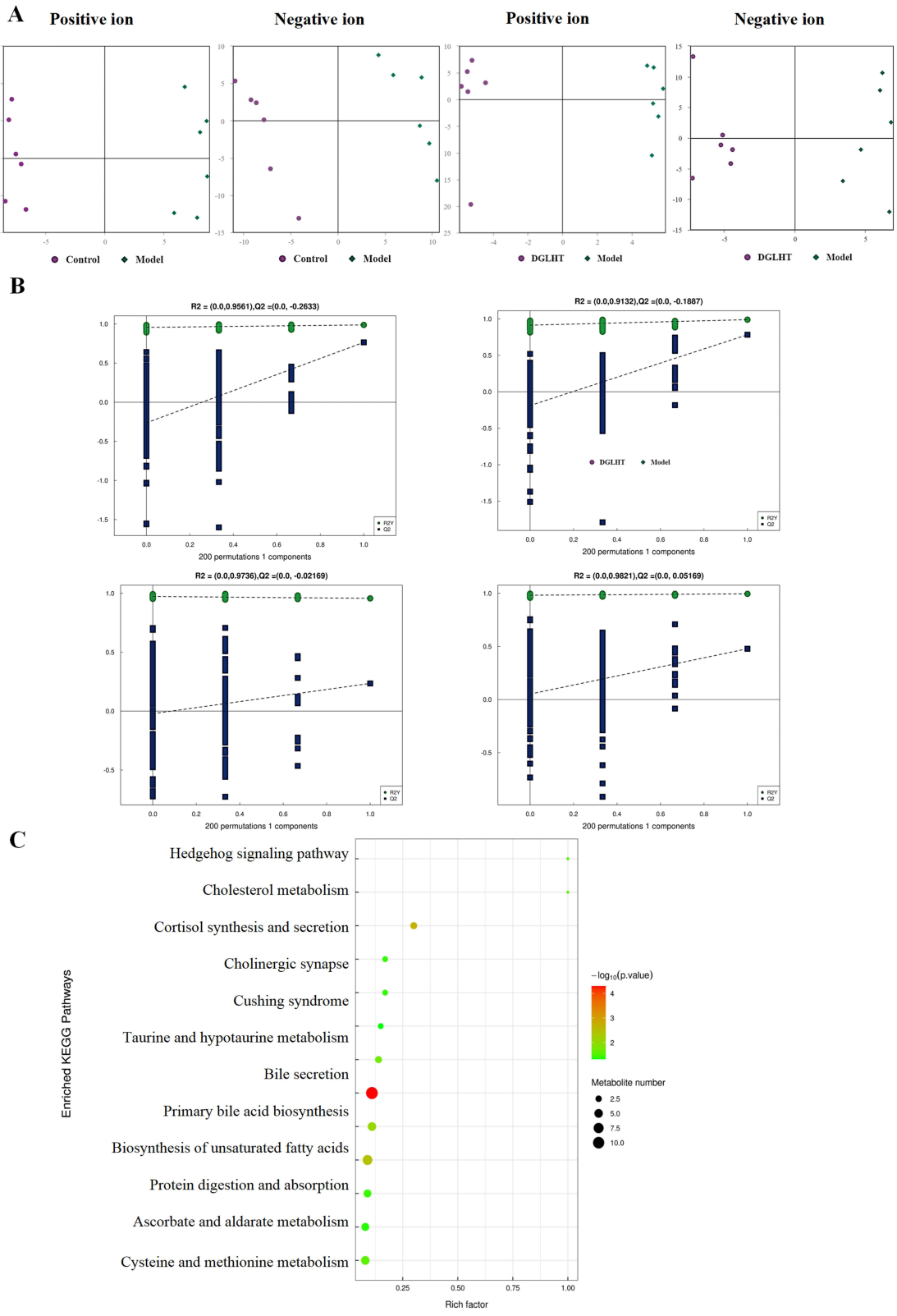

Figure 3 Effect of DGLHT metabolites in T2DM mice (n=6). (**A**) OPLS-DA plot of differential metabolites in the liver of T2DM mice. (**B**) OPLS-DA displacement test of differential metabolites in the liver of T2DM mice. (**C**) The KEGG pathway is enriched in the liver of T2DM mice.

Table 1 Differential Metabolites

Mode	Name	m/z	t_R(s)	P value	VIP	Con. vs. Mod.	Mod. vs DGLHT
ESI^-	Palmitic acid	255.2331	52.5040	0.0007	25.9977	Down	–
	Taurodeoxycholic acid	498.2889	162.4670	0.0468	23.6568	Up	–
	Cis-4,7,10,13,16,19-docosahexaenoic acid	327.2320	49.4255	0.0216	22.6821	Down	–
	Pe(16:1e/10-hdohe)	762.5079	150.2450	0.0061	15.2288	Down	–
	Cholesteryl sulfate	465.3048	29.7120	0.0242	13.3535	Up	–
	1-oleoyl-sn-glycero-3-phosphoethanolamine	478.2923	206.4395	0.0313	10.8236	Up	–
	Deoxycholic acid	391.2831	172.2465	0.0014	9.9332	Up	–
	Eicosenoic acid	309.2779	47.2730	0.0008	7.9644	Up	–
	Eicosapentaenoic Acid	301.2150	48.7600	0.0044	6.5124	Down	–
	Propanoic acid, 2-[[4-[2-[[[(cyclohexylamino)carbonyl](4-cyclohexylbutyl)amino]ethyl]phenyl]thio]-2-methyl-	501.3184	115.4660	0.0103	6.0094	Down	–
	13s-hydroperoxy-9z,11e-octadecadienoic acid	293.2104	58.3400	0.0088	5.4880	Down	–
	Lumichrome	241.0724	66.3335	0.0179	5.353	Down	–
	Pc(16:0e/11,12-epete)	840.5747	147.3745	0.0013	4.3561	Down	–
	gamma-linolenic acid	277.2154	50.4630	0.0176	9.0077	–	Down
	1-palmitoyl-2-hydroxy-sn-glycero-3-phospho-(1′-rac-glycerol)	483.2702	170.9055	0.0022	6.0318	–	Down
	Dl-lactate	89.0250	278.0210	0.0254	8.3246	–	Up
	Histidine	154.0616	481.0800	0.0194	4.0840	–	Up
	Indoxyl sulfate	212.0010	32.6530	0.0168	3.8411	–	Down
	Linoleic acid	279.2330	48.2565	0.0347	28.0188	–	Down
	Oxyresveratrol	487.1281	169.6340	0.0178	3.6281	–	Down
	Pseudouridine	243.0620	171.4095	0.0156	15.8173	–	Down
ESI^+	1-Stearoyl-sn-glycerol 3-phosphocholine	546.3516	191.0180	0.0027	10.4030	Down	–
	Betaine	118.0865	289.8060	0.0034	8.3430	Up	–
	Hypoxanthine	137.0449	183.8575	0.0376	7.6656	Up	–
	6-[3-[(3,4-dimethoxyphenyl)methyl]-4-methoxy-2-(methoxymethyl)butyl]-4-methoxy-1,3-benzodioxole	415.1954	38.1985	0.0125	5.8786	Up	–
	Sphingosine	282.2774	115.6180	0.0407	5.5663	Down	–
	1-palmitoyl-2-stearoyl-sn-glycero-3-phosphocholine	784.5791	65.1310	0.0329	4.6185	Down	–
	Erucamide	338.3410	35.6345	0.0338	5.8971	–	Down
	Hypoxanthine	137.0449	183.8575	0.0228	11.2401	–	Down

Notes: ESI^-: negative ion mode. ESI^+: positive ion mode. Up: The compound is upregulated. Down: The compound is downregulated.

β-diversity analysis assesses the similarity of gut microbiota between groups. In the Model group, Bray-Curtis and Weighted Unifrac indices increased, while the Unweighted Unifrac index decreased compared to the Control group. Following DGLHT intervention, the Unweighted Unifrac index increased, and both Bray-Curtis and Weighted Unifrac indices decreased compared to the Model group (Figure 5B).

After identifying operational taxonomic units (OTUs) with a 97% similarity threshold, analyzing common and unique OTUs among each group, and constructing a Venn diagram, it was observed that the Control group and Model group, as well as the DGLHT group and Model group, were both classified into the same OTUs with 293 and 325 OTUs, respectively. Based on species annotation results, the top 10 species with the highest abundance ranking at each classification level (Phylum, Class, Order, Family, Genus, and Species) were selected for each group, and a bar chart of relative species abundance was generated. At the Phylum level, *Actinobacteria* abundance increased, while *Bacteroidota* abundance decreased in both the Model and DGLHT groups compared to the Control group. *Proteobacteria* and *Actinobacteria* levels rose following DGLHT intervention. At the Class level, *Bacilli* abundance increased and *Bacteroidia* abundance decreased across all groups compared to the Control. At the Order level, *Bifidobacteria* abundance increased significantly, and *Bacteroidales* abundance decreased significantly in all groups compared to the Control. At the family level, *Muribaculaceae* abundance decreased significantly. At the Genus level, *Lachnospiraceae* showed no significant change, while *Lactobacillus* decreased and *Dubosiella* increased

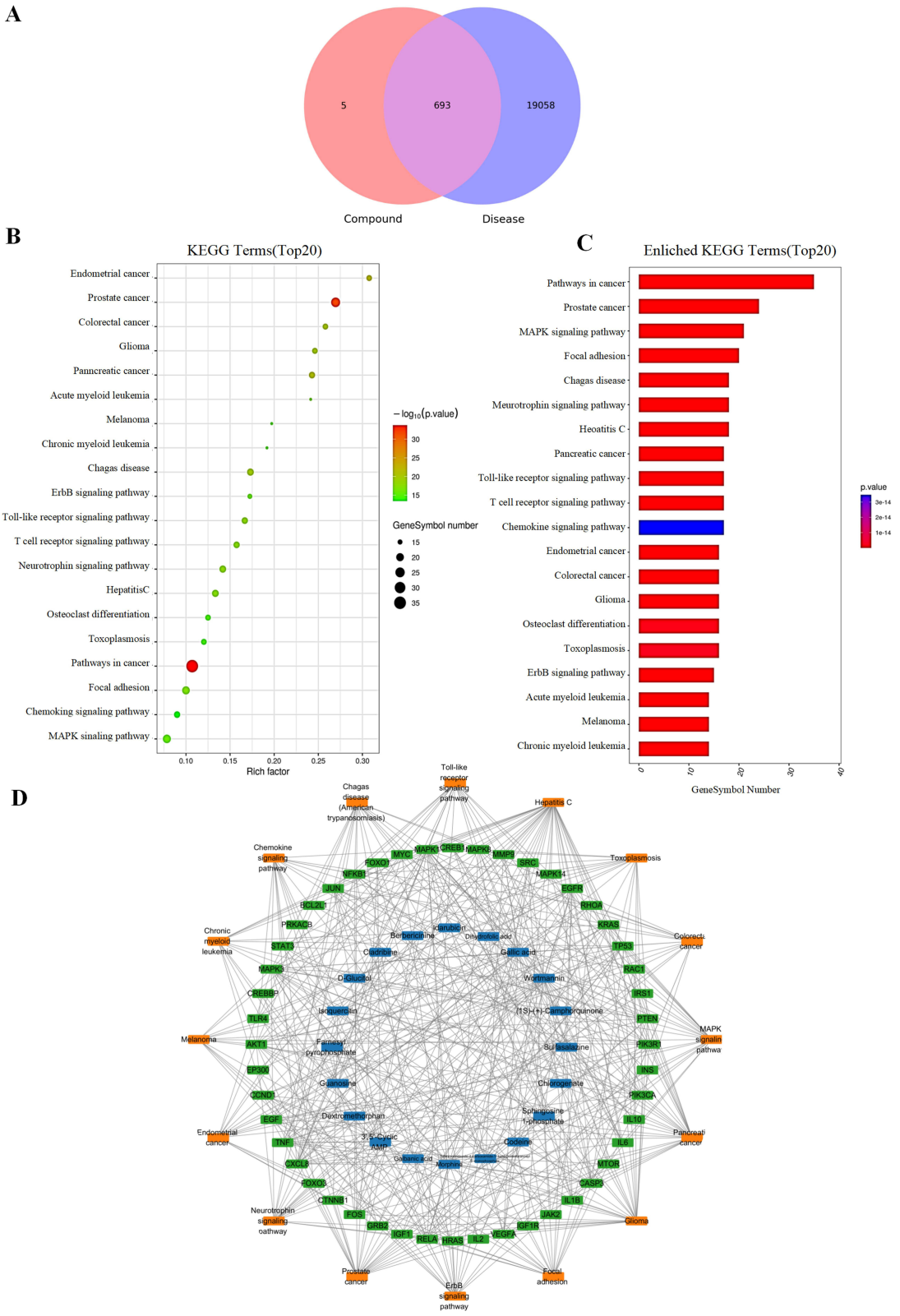

Figure 4 Network diagram of DGLHT in treating T2DM. (**A**) Venn diagram of traditional Chinese medicine and disease targets in the treatment of T2DM with DGLHT. (**B**) KEGG Pathway TOP20 Bubble Chart of DGLHT in the Treatment of T2DM. (**C**) Enrichment analysis of KEGG pathway TOP20 in the treatment of T2DM with DGLHT. (**D**) DGLHT for the treatment of T2DM components targets disease diagram.

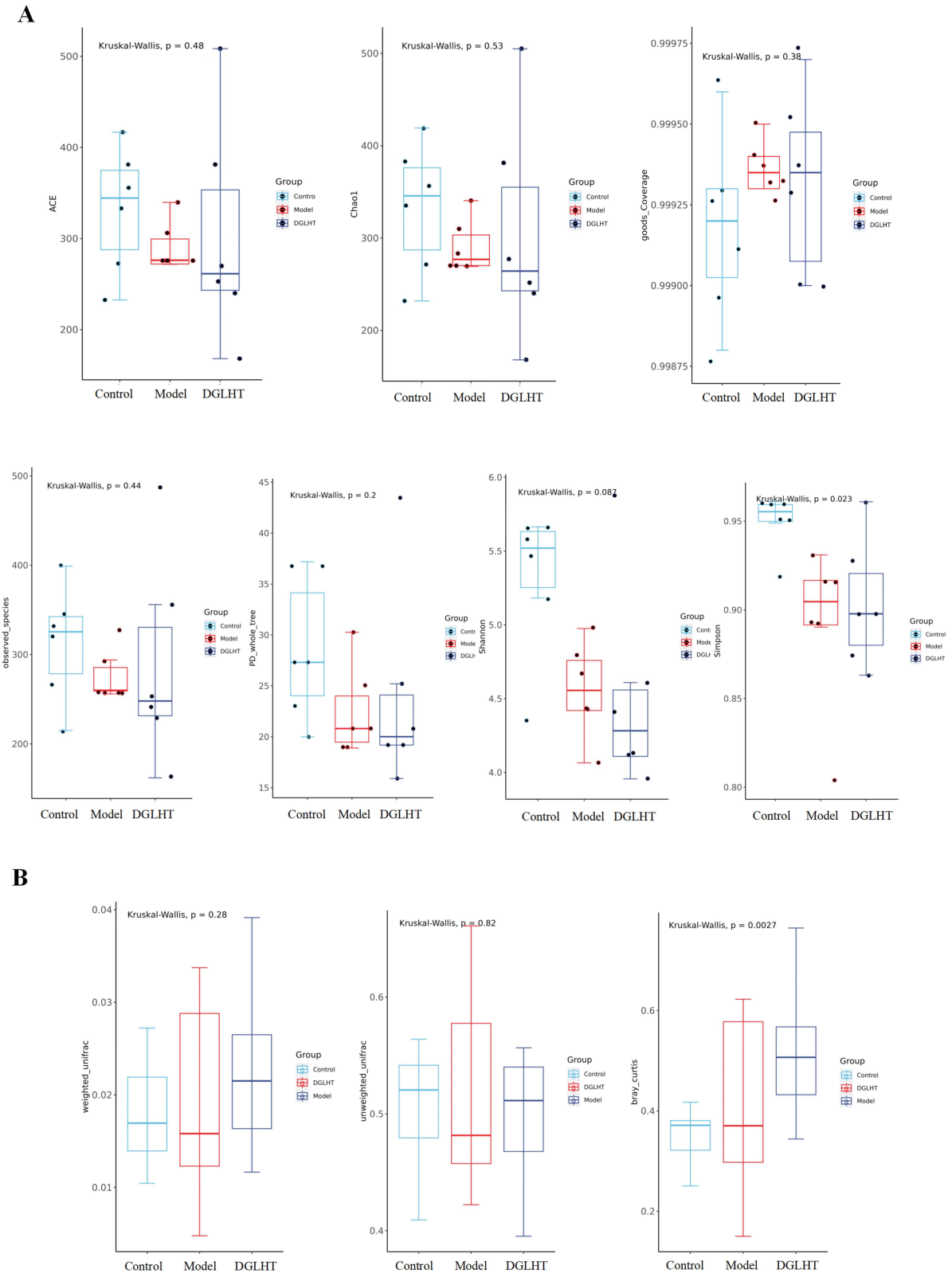

Figure 5 The effect of DGLHT on gut microbiota in T2DM mice. (**A**) Analysis of alpha diversity in gut microbiota. (**B**) Beta diversity map of gut microbiota.

https://doi.org/10.2147/DMSO.S525913

significantly after DGLHT intervention. At the Species level, *Cyanobacteria* abundance did not differ significantly among the groups (Figure 6A).

STAMP analysis revealed significant differences in the microbial communities at the genus level, specifically *Muribaculaceae* and *Enterorhabdus*, among the Model, DGLHT, and Control groups (Figure 6B). KEGG functional prediction indicates that DGLHT influences carbohydrate metabolism, intestinal membrane transport, and amino acid metabolism in mice (Figure 7A).

Correlation Analysis

A Spearman correlation hierarchical clustering analysis on the microbiota, compound components, and components with significant differences revealed that the bacterial genus *Candidatus Saccharimonas*, the compound Bayin, and the components Linoleic acid and gamma-Linolenic acid exhibited the strongest correlations before and after DGLHT administration (Figure 7B).

DGLHT Affects the Protein Expression of the TLR4/NF-κB/NLRP3 Pathway in Liver Tissue of T2DM Mice

To assess the impact of DGLHT on liver protein expression in T2DM mice, the expression levels of p-NF-κB/NF-κB, TLR4, and NLRP3 were measured in mouse liver tissue. Following DGLHT treatment, p-NF-κB (p65)/NF-κB (p65) (high-dose group $P < 0.05$; Metformin group $P < 0.01$), TLR4 (low-dose group $P < 0.05$; Metformin group $P < 0.01$), and NLRP3 (low-dose group and Metformin group $P < 0.05$) were significantly reduced. These findings indicate that DGLHT effectively alleviates the inflammatory response in T2DM mice (Figure 8).

DGLHT Affects the Expression of PI3K/AKT/GLUT4 Pathway Proteins in Liver Tissue of T2DM Mice

To assess the impact of DGLHT on protein expression in T2DM mice, the expression levels of p-PI3K/PI3K, p-AKT/AKT, and GLUT4 were measured in the mouse liver. Following DGLHT treatment, the expression level of p-AKT/AKT significantly increased in the high-dose group ($P < 0.01$), indicating that DGLHT effectively alleviates IR in T2DM mice (Figure 8).

DGLHT Affects the Expression of HO-1/SOD2/CAT Pathway Proteins in Liver Tissue of T2DM Mice

To assess the impact of DGLHT on liver protein expression in T2DM mice, the expression levels of HO-1, SOD2, and CAT were measured in mouse liver tissue. Following DGLHT treatment, the expression level of HO-1 significantly increased in the high-dose group ($P < 0.05$). Additionally, SOD2 expression was significantly reduced in the low-dose, high-dose, and Metformin groups ($P < 0.01$). These findings collectively indicate that DGLHT effectively alleviates oxidative stress levels in T2DM mice (Figure 8).

DGLHT Affects the Expression of AMPK/Sirt1/PGC-1 α Pathway Proteins in the Liver Tissue of T2DM Mice

To assess the impact of DGLHT on liver protein expression in T2DM mice, the expression levels of p-AMPK/AMPK, Sirt1, and PGC-1α were measured in mouse liver tissue. Following DGLHT treatment, the expression level of p-AMPK/AMPK significantly increased in the low-dose group ($P < 0.05$), indicating that DGLHT effectively alleviates energy metabolism in T2DM mice (Figure 8).

Discussion

T2DM, the most prevalent metabolic disease, is characterized by hyperglycemia, hyperlipidemia, and insulin resistance, leading to severe complications such as coronary and lower limb artery diseases and diabetic nephropathy, which significantly impact the quality of life.[17] Genome-wide association studies (GWAS) have revealed a significant association between T2DM and variations in gut microbiota, bacterial genes, and metabolic pathways.[18] Metabolomics technology has made substantial advancements in the field of traditional Chinese medicine in recent years. Its holistic

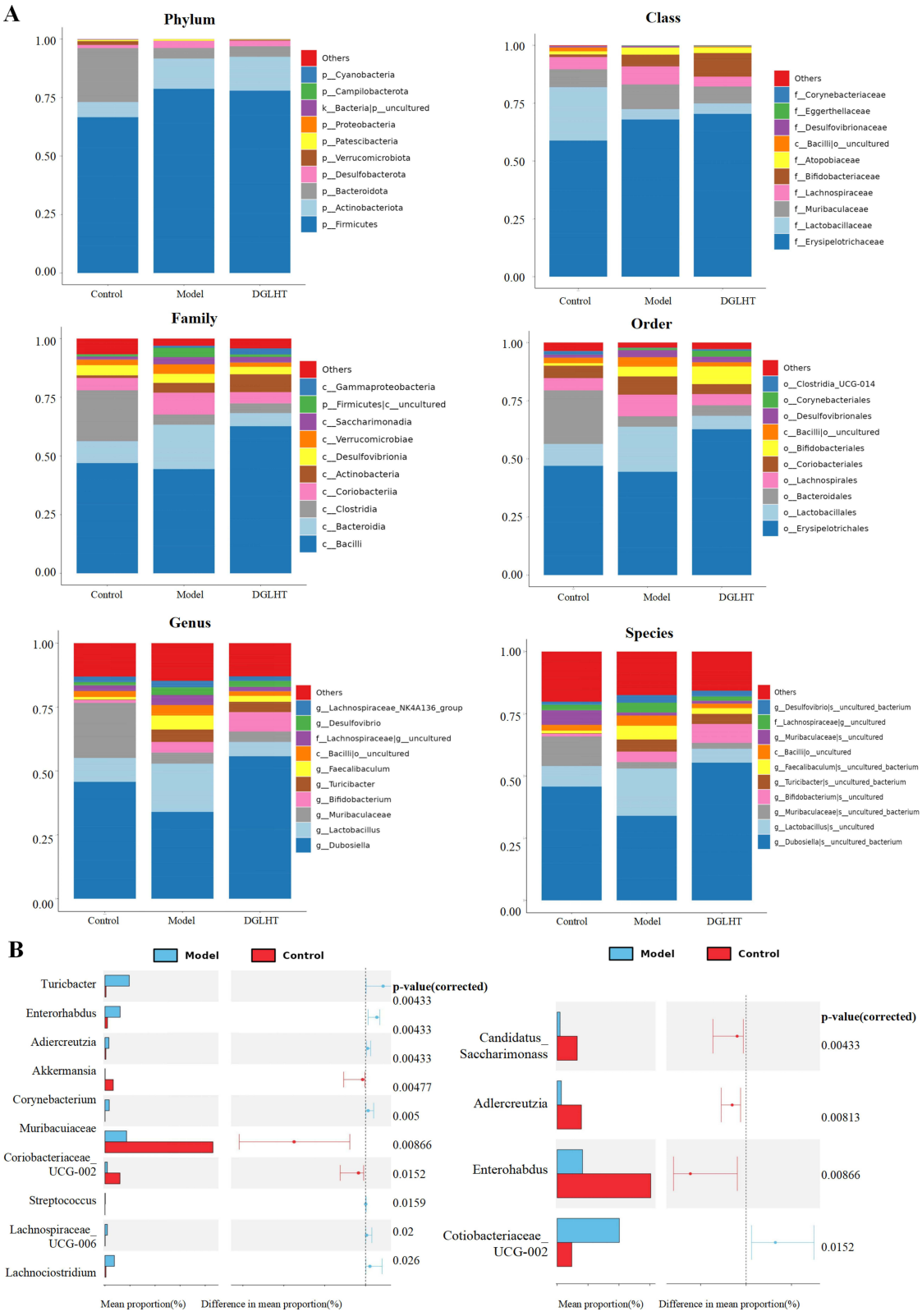

Figure 6 The effect of DGLHT on gut microbiota in T2DM mice. Bar chart analysis of inter group differences in relative abundance index of gut microbiota species (**A**). STAMP analysis of gut microbiota (**B**).

https://doi.org/10.2147/DMSO.S525913

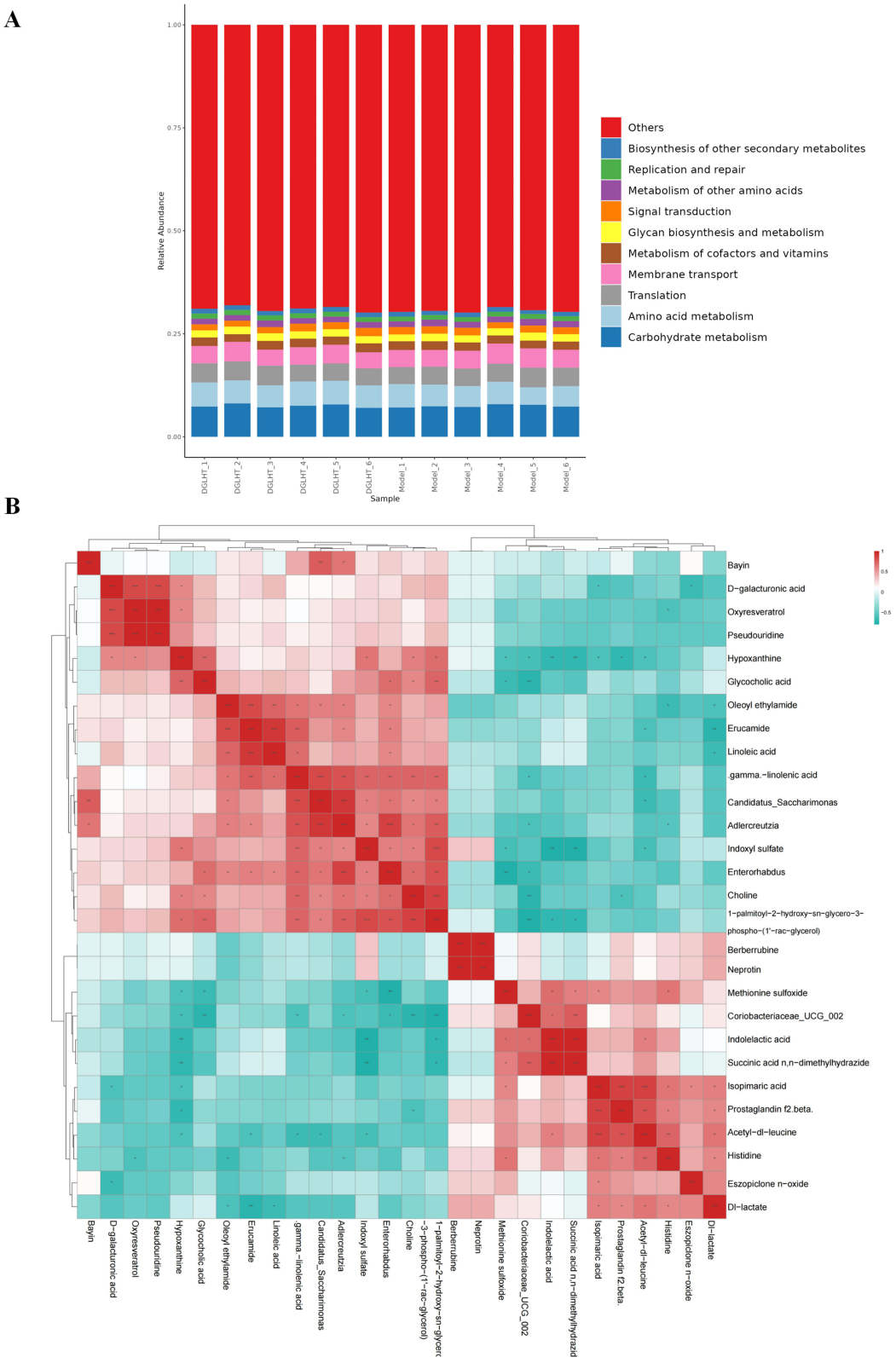

Figure 7 The effect of DGLHT on gut microbiota in T2DM mice. (**A**) KEGG prediction of gut microbiota in the treatment of T2DM with DGLHT. (**B**) Correlation analysis of differential metabolites and microbiota in the treatment of T2DM with DGLHT.

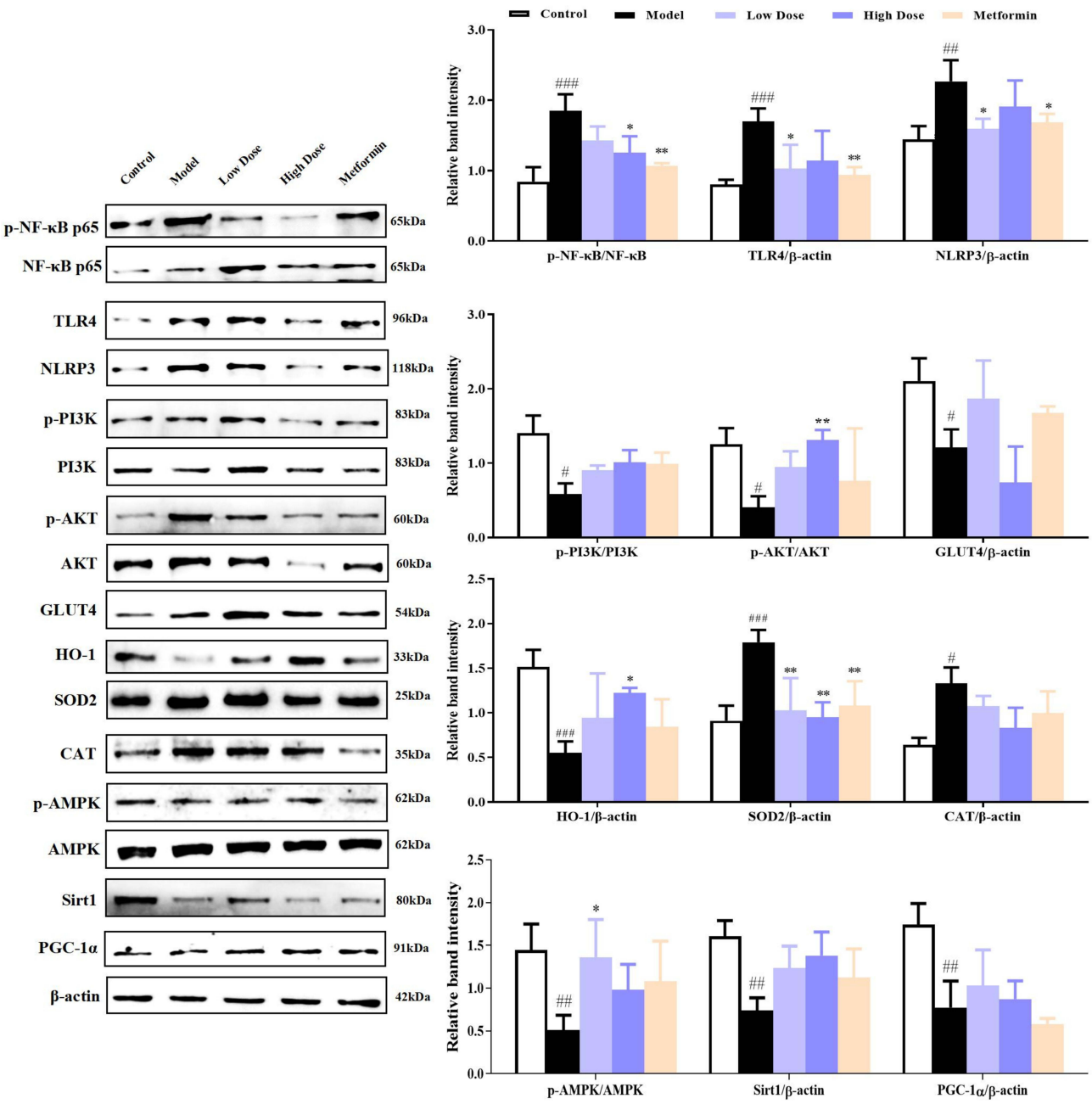

Figure 8 DGLHT's effect on liver protein expression Level in T2DM Mice.Three samples were analyzed for each group. The data were analyzed using an unpaired *t*-test. $^{\#}P<0.05$, $^{\#\#}P<0.01$, $^{\#\#\#}P<0.001$ vs Control group, $^{*}P<0.05$, $^{**}P<0.01$ vs Model group.Bar graphs show mean ± SD.

research approach aligns with the "holistic view" of traditional Chinese medicine, emphasizing the regulation of body functions through multiple targets and mechanisms. Metabolomics techniques are commonly used to identify chemical components and components, thereby validating drug mechanisms of action. This experiment investigated the material basis of DGLHT treatment for T2DM using metabolomics and 16S rRNA sequencing. Additionally, protein immunoblotting was employed to verify pathway-related protein expressions, providing valuable insights for the application of traditional Chinese medicine in T2DM treatment.

Contemporary pharmacokinetic studies indicate that the primary active constituents in the formula—such as berberine, astragaloside IV, and catalpol—generally reach steady-state plasma concentrations within 2 to 4 weeks after administration. These compounds effectively activate the AMPK/PI3K-Akt signaling pathway, which promotes

https://doi.org/10.2147/DMSO.S525913

GLUT4 translocation and enhances insulin sensitivity. As a result, Phase II clinical trials commonly adopt the 4-week time point as the primary endpoint for efficacy assessment, enabling efficient identification of potentially effective formulations.[19] A network pharmacology study revealed that the 70 bioactive constituents in DGLHT need sustained administration over a period of 3–4 weeks to effectively regulate key pathways such as glycolysis and insulin secretion via molecular targets including GAA, PRKCB, and GCK. This cumulative pharmacological effect supports the rationale for utilizing a 4-week observation window in efficacy evaluations.[20] Current protocols involve the addition of herbal medicine to established conventional hypoglycemic regimens. A 4-week evaluation period is recommended to minimize glycemic fluctuations that may confound the assessment of treatment efficacy.[21] Extended monitoring primarily focuses on the prevention and management of diabetic complications, including improvements in vascular endothelial function.[12] DGLHT includes Angelicae Sinensis Radix, Radix Rehmanniae, Rehmanniae Radix Praeparata, Scutellariae Radix, Coptidis Rhizoma, Phellodendri Chinensis Cortex, and Astragali Radix, which exhibit properties such as heat-clearing, yin-tonifying, anti-liver fibrosis, inhibition of pancreatic islet cell apoptosis, and immune suppression. DGLHT contains Ferulic acid, Rehmannin D, and other components that can promote glucose uptake by HepG2 cells, inhibit T lymphocyte proliferation, promote the differentiation of regulatory T cells (Tregs) in vivo, inhibit the interaction between dendritic cells (DCs) and T lymphocytes, increase the expression of programmed death ligand 1, reduce the percentage of dendritic cell subsets of proliferating cells, thereby reducing T-cell-mediated inflammation and improving diabetes.[22] Our experiment confirmed the presence of Ferulic acid and Rehmannin D within DGLHT, both of which harbor anti-inflammatory properties that can alleviate IR and treat diabetes complications.[23] The liver, as the body's primary metabolic organ, demonstrates remarkable regenerative and self-repair capabilities. Each hepatocyte contains approximately 1000 to 2000 mitochondria.[24] Mitochondria, which are critical for metabolic regulation in organisms, produce ATP by breaking down macronutrients—such as carbohydrates, proteins, and lipids—to sustain cellular functions and maintain energy homeostasis. Dysfunction of mitochondria, manifested as impaired insulin secretion from pancreatic β-cells and IR, plays a key role in the development of diabetes.[25] Thus, quantifying hepatic protein expression serves as a key indicator for evaluating mitochondrial function.

Research has demonstrated that the pathogenesis of liver injury in T2DM involves various factors, such as glucose and lipid metabolism disorders, inflammatory reactions, and oxidative stress.[26] Low-grade inflammatory response has been identified as a key mediator in the development of IR, activating TLR4 to induce NF-κB-mediated secretion of inflammatory cytokines,[27] including tumor necrosis factor-alpha (TNF-α), interleukin-1 beta (IL-1β), and interleukin-18 (IL-18), which subsequently affect the transactivation of the insulin signaling pathway. TLR4 activates NF-κB and downstream pro-inflammatory cytokines through signal transduction, triggering inflammatory responses.[28] Inhibiting TLR4 expression can reduce NF-κB activation, thereby mitigating inflammatory responses. The production of NLRP3 is dependent on the NF-κB pathway and plays a crucial role in the inflammatory response. As an important regulatory factor upstream of the inflammatory pathway, NLRP3 participates in the occurrence and development of diabetes. Inhibiting NLRP3 inflammasome activation can significantly suppress the cascade amplification of downstream inflammatory pathways, improving the progression and prognosis of related inflammatory diseases. This study indicates that DGLHT significantly ameliorates inflammation in T2DM mice by modulating the TLR4/NF-κB/NLRP3 pathway.[29]

Poorly managed diabetes and related metabolic disorders, such as impaired lipid metabolism, oxidative stress, and hypertension, can lead to microvascular and macrovascular complications.[30] IR is the primary factor contributing to T2DM. Once IR occurs, the body's glucose uptake and utilization decrease, leading to a continued rise in blood glucose levels. The body's compensatory secretion of excessive insulin results in hyperinsulinemia, which further contributes to the occurrence and development of diabetes. Factors that cause IR include central nervous system inflammation, increased inflammation mediated by macrophages, activation of the tumor necrosis factor pathway, changes in mitochondrial dynamics, elevated levels of circulating fatty acids, and lipid accumulation in muscles and liver.[31–33] The liver, the largest endocrine organ in the human body, is a primary target organ for insulin action. In T2DM patients, the inhibitory effect of insulin on liver cell glucose production is disrupted, leading to increased IR and elevated blood glucose levels. The insulin-mediated PI3K/AKT pathway regulates glucose and lipid metabolism by modulating effector factors related to metabolism, such as GLUT4. GLUT4 promotes the ability of cells in insulin-sensitive tissues to uptake glucose, thereby improving IR symptoms.[34] Conversely, the absence of GLUT4 can also lead to IR. Our study demonstrates that

DGLHT improves T2DM by reducing OGTT and ITT levels, potentially through the amelioration of IR via the PI3K/AKT/GLUT4 signaling pathway.[35]

The stimulation of inflammatory factors can also lead to excessive production of reactive oxygen species (ROS), causing liver damage. Specifically, the excessive production of lipid peroxidation substance malondialdehyde (MDA) consumes SOD and CAT, which possess antioxidant and free radical scavenging abilities, resulting in an imbalance of the body's antioxidant system and oxidative stress.[36] This study indicates that DGLHT alleviates liver oxidative stress and improves liver damage in T2DM mice to varying degrees through the HO-1/SOD2/CAT pathway. During the oxidative stress process induced by high glucose environment stimulation, downregulation of SIRT1/PGC-1α expression was detected, leading to a reduction in mitochondrial oxidative energy supply in related cells. This can cause damage to skeletal muscle and other cells, exacerbate glucose metabolism disorders, and accelerate the progression of complications such as obesity. Research has shown that SIRT1 is an important regulatory factor in liver fat production and fat oxidation, capable of regulating AMPK activation. Activated AMPK inhibits liver fat production and stimulates fat oxidation, thereby regulating cellular lipid metabolism processes. As the most representative factor of the Sirtuins protein family, SIRT1 is located in the nucleus and has deacetylase activity.[37] Its acetylation can act on histones, transcription regulators, or other proteins to modify and regulate gene expression. SIRT1 exhibits various biological regulatory effects, including inhibiting cell apoptosis, regulating energy metabolism, and exerting anti-inflammatory and antioxidant stress regulation. Multiple studies have demonstrated that stimulating the normal expression of SIRT1 can not only alleviate cell damage and apoptosis but also regulate various related signaling pathways such as energy metabolism, thereby maintaining the normal function of cells and organs.[38,39] This study indicates that DGLHT alleviates liver energy metabolism in T2DM mice to varying degrees through the AMPK/Sirt1/PGC-1α pathway, as evidenced by the significant increase in p-AMPK/AMPK expression levels in the low-dose group.

The gut microbiota interacts with host metabolism and immune function. Human health and diet influence gut microbiota composition, affecting metabolism.[40,41] Numerous studies have indicated a strong association between changes in gut microbiota and diabetes development. *Bacteroides*/*Firmicutes* probiotics are linked to increased intestinal permeability, allowing bacterial by-products to enter and trigger diabetes-related inflammation.[42] Consequently, this leads to IR, which is characterized by impaired ITT and fasting hyperglycemia. Candidatus_Saccharimonas is a common symbiotic bacterium found in the oral cavity of healthy individuals. It can cause opportunistic fungal infections, and the immune function of patients with diabetes is often reduced, frequently accompanied by oral Candida infection. Some studies have also demonstrated a correlation between blood sugar levels and Candida, which is further confirmed by this study.[43] DGLHT is rich in alkaloids and flavonoids, which directly inhibit Candida proliferation by disrupting fungal membrane integrity and suppressing hyphal formation, thereby reducing infection-associated glycemic fluctuations and enhancing disease management.[44] Patients with T2DM often exhibit compromised immune function, rendering them susceptible to opportunistic infections such as Candidiasis. Notably, such infections and associated inflammatory responses can exacerbate glycemic fluctuations, thereby establishing a vicious cycle. Alkaloids and flavonoids have been demonstrated to directly suppress the overgrowth of conditional pathogens, including Candida species. By inhibiting these pathogenic microorganisms, this cycle is effectively disrupted, thereby fostering a microenvironment conducive to glycemic stability.

Angelica and Astragalus polysaccharides promote the proliferation of probiotics, thereby enhancing intestinal barrier function, reducing gut permeability, and increasing short-chain fatty acid (SCFA) production, which collectively contribute to stabilizing the gut microbiota. Astragalus polysaccharides and Angelica polysaccharides have been demonstrated to selectively promote the proliferation of probiotics such as *Bifidobacterium* and *Lactobacillus*. These probiotics enhance intestinal barrier function, reduce endotoxin translocation, mitigate systemic inflammation at its source, and consequently improve insulin sensitivity and FBG levels.[45] Patients with T2DM exhibit a significant reduction in the abundance of SCFA-producing bacteria, particularly butyrate-producing species, whose decline is closely associated with insulin resistance and deteriorated glycemic control. SCFAs serve not only as an energy source for intestinal epithelial cells but also enter systemic circulation to exert effects on hepatic and peripheral tissues.[46] Through activation of G protein-coupled receptors and inhibition of histone deacetylases, SCFAs promote glucose uptake and fatty acid oxidation, thereby enhancing insulin sensitivity and improving ITT and OGTT. The polysaccharide components in

DGLHT provide ample fermentation substrates for SCFA-producing microbiota, significantly elevating intestinal SCFA levels and thereby beneficially regulating host metabolism. Through gradual release within the intestinal lumen, DGLHT markedly increases the abundance of Akkermansia, which confers beneficial effects through multiple mechanisms including enhancement of mucus layer thickness, improvement of intestinal barrier integrity, and modulation of immune-inflammatory responses. During decoction, baicalin and berberine form hydrophobic complexes that precipitate and subsequently dissociate gradually in the intestine, prolonging the retention time of bioactive compounds and significantly increasing the abundance of Akkermansia.[47]

The results indicate that DGLHT effectively manages T2DM by lowering blood glucose levels, thereby supporting the initial research hypothesis. Furthermore, DGLHT exhibits potential in intervening in chronic pre-diabetic conditions. However, its clinical application should strictly follow the principles of TCM syndrome differentiation, particularly for patients diagnosed with the yin deficiency with effulgent fire pattern. While DGLHT shows promise in diabetes prevention and may offer tailored therapeutic benefits across different stages of the disease, further investigation through stage-specific clinical trials is warranted. It is important to note that translating findings from murine models into clinical practice is complicated by factors such as comorbidities and polypharmacy. Patients with clinical T2DM often present with concurrent conditions like hypertension, dyslipidemia, or obesity, requiring combination therapies involving antihypertensive agents, statins, or antiplatelet drugs, which may influence treatment outcomes.[48] The monodisease-state animal model utilized in this study limited the evaluation of DGLHT's interactions with conventional pharmacotherapies. Moreover, substantial metabolic heterogeneity is present in human T2DM, with approximately 20–30% of refractory cases exhibiting endogenous hypercortisolism that aggravates insulin resistance—a specific endocrine subphenotype that cannot be recapitulated in animal models. Therefore, the translation of findings into clinical practice necessitates comedication strategies guided by therapeutic outcomes.

The clinical application of DGLHT for T2DM requires strict adherence to prescribed protocols, including compliance with the recommended treatment duration and dietary guidelines. Patients should undergo weekly monitoring of both fasting and postprandial blood glucose levels. Conventional medications must be continued as prescribed without self-discontinuation, particularly during combination therapy, which necessitates intensified glycemic monitoring to prevent hypoglycemia. Concurrently, lifestyle modifications should emphasize the consumption of low-glycemic-index foods, avoidance of high-glycemic-index items, engagement in appropriate physical activity to improve IR, and maintenance of sufficient sleep to enhance insulin sensitivity.

Conclusion

DGLHT demonstrates remarkable therapeutic potential in the management of T2DM by ameliorating IR through multiple interconnected pathways, such as modulating inflammatory responses, optimizing energy metabolism, and mitigating oxidative stress. By influencing the body's metabolic processes and reshaping the composition of gut microbiota, DGLHT lays a solid foundation for clinical interventions and offers promising prospects for effective diabetes therapy.

Data Sharing Statement

The datasets supporting the conclusions of this article are included within the article. Further inquiries can be addressed to the corresponding author.

Ethics Approval and Consent to Participate

The authors report no conflicts of interest in this work. The Ethics Committee of Shanxi University of Chinese Medicine granted exemption from review for available data from public databases involving in our research. The animal experiments conducted in this study were approved by the Animal Ethics Committee of Shanxi University of Chinese Medicine (approval no. 2022DW087).

Funding

The authors declare that financial support was received for the research, authorship, and/or publication of this article. Financial support from the projects of Shanxi Province (No.2025L075, No.20230034, No.2023-156, No.2023ZYYA2012, No.20210302124694 and No.2021L364), the Science and Technology Innovation Ability Cultivation Program Projects of Shanxi University of Chinese Medicine (No.2023BK38, No.2022PY-TH-02, No.2024PY-JL-7-02 and No.2022JD-KF-04), the project of Shanxi Key Laboratory of Traditional Herbal Medicines Processing (No. 202104010910029), the Innovation Team of Shanxi University of Chinese Medicine (No. 2022TD1014), and the Discipline Construction of Shanxi University of Chinese Medicine (No.2025XK34).

Disclosure

The authors have declared no conflicts of interest in this work.

References

1. Pedersen HK, Gudmundsdottir V, Nielsen HB, et al. Human gut microbes impact host serum metabolome and insulin sensitivity. *Nature*. 2016;535(7612):376–381. doi:10.1038/nature18646
2. Lovic D, Piperidou A, Zografou I, Grassos H, Pittaras A, Manolis A. The growing epidemic of diabetes mellitus. *Curr Vasc Pharmacol*. 2020;18(2):104–109. doi:10.2174/1570161117666190405165911
3. American Diabetes Association. 2. Classification and diagnosis of diabetes: standards of medical care in diabetes-2018. *Diabetes Care*. 2018;41(Suppl 1):S13–s27. doi:10.2337/dc18-S002
4. Ogurtsova K, da Rocha Fernandes JD, Huang Y, et al. IDF Diabetes Atlas: global estimates for the prevalence of diabetes for 2015 and 2040. *Diabetes Res Clin Pract*. 2017;128:40–50. doi:10.1016/j.diabres.2017.03.024
5. Schmidt AM. Highlighting diabetes mellitus: the epidemic continues. *Arteriosclerosis Thrombosis Vasc Biol*. 2018;38(1):e1–e8. doi:10.1161/ATVBAHA.117.310221
6. Zheng Y, Ley SH, Hu FB. Global aetiology and epidemiology of type 2 diabetes mellitus and its complications. *Nat Rev Endocrinol*. 2018;14(2):88–98. doi:10.1038/nrendo.2017.151
7. Guardado-Mendoza R, Salazar-López SS, Álvarez-Canales M, et al. The combination of linagliptin, metformin and lifestyle modification to prevent type 2 diabetes (PRELLIM). A randomized clinical trial. *Metabolism*. 2020;104:154054. doi:10.1016/j.metabol.2019.154054
8. Song Z, Yang R, Wang W, et al. Association of healthy lifestyle including a healthy sleep pattern with incident type 2 diabetes mellitus among individuals with hypertension. *Cardiovasc Diabetol*. 2021;20(1):239. doi:10.1186/s12933-021-01434-z
9. Meng X, Liu X, Tan J, et al. From Xiaoke to diabetes mellitus: a review of the research progress in traditional Chinese medicine for diabetes mellitus treatment. *ChinMed*. 2023;18(1):75. doi:10.1186/s13020-023-00783-z
10. Liu T, Cao H, Ji Y, et al. Interaction of dendritic cells and T lymphocytes for the therapeutic effect of Dangguiliuhuang decoction to autoimmune diabetes. *Sci Rep*. 2015;5:13982. doi:10.1038/srep13982
11. Meng X, Liu X, Chen N. Differential mechanism of action of raw and processed Rehmannia rehmannia mediated NF-κB/NLRP3 signaling pathway in high-fat diet and streptozotocin-induced diabetic mice. *Chin J Trad Chin Med*. 2021;46(21):5627–5640. doi:10.19540/j.cnki.cjcmm.20210323.302
12. Xu Y, Sha W, Lu J, et al. Danggui Liuhuang Decoction ameliorates endothelial dysfunction by inhibiting the JAK2/STAT3 mediated inflammation. *J Ethnopharmacol*. 2025;340:119170. doi:10.1016/j.jep.2024.119170
13. Karczewski KJ, Snyder MP. Integrative omics for health and disease. *Nat Rev Genet*. 2018;19(5):299–310. doi:10.1038/nrg.2018.4
14. Karbasforooshan H, Karimi G. The role of SIRT1 in diabetic cardiomyopathy. *Biomed Pharmacother*. 2017;90:386–392. doi:10.1016/j.biopha.2017.03.056
15. Chen W, Wen L, Bao Y, et al. Gut flora disequilibrium promotes the initiation of liver cancer by modulating tryptophan metabolism and up-regulating SREBP2. *Proc Natl Acad Sci USA*. 2022;119(52):e2203894119. doi:10.1073/pnas.2203894119
16. Hankittichai P, Lou HJ, Wikan N, Smith DR, Potikanond S, Nimlamool W. Oxyresveratrol inhibits IL-1β-induced inflammation via suppressing AKT and ERK1/2 activation in human microglia, HMC3. *Int J Mol Sci*. 2020;21(17):6054. doi:10.1073/pnas.2203894119
17. Sung KC, Lee MY, Kim YH, et al. Obesity and incidence of diabetes: effect of absence of metabolic syndrome, insulin resistance, inflammation and fatty liver. *Atherosclerosis*. 2018;275:50–57. doi:10.1016/j.atherosclerosis.2018.05.042
18. Vallianou NG, Stratigou T, Tsagarakis S. Microbiome and diabetes: where are we now? *Diabetes Res Clin Pract*. 2018;146:111–118. doi:10.1016/j.diabres.2018.10.008
19. Feng S, Wang J, Peng Q, et al. Schisandra sphenanthera extract modulates sweet taste receptor pathway, IRS/PI3K, AMPK/mTOR pathway and endogenous metabolites against T2DM. *Phytomedicine*. 2025;136:156348. doi:10.1016/j.phymed.2024.156348
20. Peng X, Xu H, Chen H, et al. Network pharmacology-based analysis of the mechanism of Danggui Liuhuang Decoction in treating diabetes mellitus. *Tradit Chin Drug Res Clin Pharmacol*. 2019;30(08):952–958. doi:10.19378/j.issn.1003-9783.2019.08.010
21. Zhang Q, Zheng C, Han R, et al. Clinical efficacy of modified Danggui Liuhuang Decoction in treating type 2 diabetic ketoacidosis. *J Chin Med Crit Care*. 2021;30(05):855–857. doi:10.19879/j.cnki.1004-745X.2021.05.032
22. Gao Z, Li Q, Wu X, Zhao X, Zhao L, Tong X. New insights into the mechanisms of Chinese herbal products on diabetes: a focus on the "Bacteria-Mucosal Immunity-Inflammation-Diabetes" Axis. *J Immunol Res*. 2017;2017:1813086. doi:10.1155/2017/1813086
23. Magee C, Grieve DJ, Watson CJ, Brazil DP. Diabetic nephropathy: a tangled web to unweave. *Cardiovasc Drugs Ther*. 2017;31(5–6):579–592. doi:10.1007/s10557-017-6755-9

24. Chen P, Yao L, Yuan M, et al. Mitochondrial dysfunction: a promising therapeutic target for liver diseases. *Genes Dis*. 2023;11(3):101115. doi:10.1016/j.gendis.2023.101115
25. Yu J, Du Y, Ji X, et al. Research progress on mechanisms of traditional Chinese medicine in treating type 2 diabetes complicated with liver injury. *Chin Tradit Herbal Drugs*. 2025;56(06):2214–2223.
26. Nawrot M, Peschard S, Lestavel S, Staels B. Intestine-liver crosstalk in type 2 diabetes and non-alcoholic fatty liver disease. *Metabolism*. 2021;123:154844. doi:10.1016/j.metabol.2021.154844
27. Zhang H, Gao X, Li K, et al. Sandalwood seed oil ameliorates hepatic insulin resistance by regulating the JNK/NF-κB inflammatory and PI3K/AKT insulin signaling pathways. *Food Funct*. 2021;12(5):2312–2322. doi:10.1039/d0fo03051a
28. Dasu MR, Devaraj S, Zhao L, Hwang DH, Jialal I. High glucose induces toll-like receptor expression in human monocytes: mechanism of activation. *Diabetes*. 2008;57(11):3090–3098. doi:10.2337/db08-0564
29. Mangan MSJ, Olhava EJ, Roush WR, Seidel HM, Glick GD, Latz E. Targeting the NLRP3 inflammasome in inflammatory diseases. *Nat Rev Drug Discov*. 2018;17(9):688. doi:10.1038/nrd.2018.149
30. Iwasaki H, Yagyu H, Shimano H. A comprehensive analysis of diabetic complications and advances in management strategies. *J Atheroscler Thromb*. 2025;32(5):550–559. doi:10.5551/jat.65551
31. Ferracini M, Martins JO, Campos MR, Anger DB, Jancar S. Impaired phagocytosis by alveolar macrophages from diabetic rats is related to the deficient coupling of LTs to the Fc gamma R signaling cascade. *Mol Immunol*. 2010;47(11–12):1974–1980. doi:10.1016/j.molimm.2010.04.018
32. Hammerschmidt P, Ostkotte D, Nolte H, et al. CerS6-derived sphingolipids interact with Mff and promote mitochondrial fragmentation in obesity. *Cell*. 2019;177(6):1536–1552.e1523. doi:10.1016/j.cell.2019.05.008
33. Li C, He JZ, Zhou XD, Xu X. Berberine regulates type 2 diabetes mellitus related with insulin resistance. *China J Chin Mater Med*. 2017;42 (12):2254–2260. doi:10.19540/j.cnki.cjcmm.20170307.014
34. Sano H, Eguez L, Teruel MN, et al. Rab10, a target of the AS160 Rab GAP, is required for insulin-stimulated translocation of GLUT4 to the adipocyte plasma membrane. *Cell Metab*. 2007;5(4):293–303. doi:10.1016/j.cmet.2007.03.001
35. DeFronzo RA, Tripathy D. Skeletal muscle insulin resistance is the primary defect in type 2 diabetes. *Diabetes Care*. 2009;32(Suppl 2):S157–163. doi:10.2337/dc09-S302
36. Singh V, Ubaid S. Role of Silent Information Regulator 1 (SIRT1) in regulating oxidative stress and inflammation. *Inflammation*. 2020;43 (5):1589–1598. doi:10.1007/s10753-020-01242-9
37. Yin Y, Wu X, Peng B, et al. Curcumin improves necrotising microscopic colitis and cell pyroptosis by activating SIRT1/NRF2 and inhibiting the TLR4 signalling pathway in newborn rats. *Innate Immun*. 2020;26(7):609–617. doi:10.1177/1753425920933656
38. Sayed AM, Hassanein EHM, Salem SH, Hussein OE, Mahmoud AM. Flavonoids-mediated SIRT1 signaling activation in hepatic disorders. *Life Sci*. 2020;259:118173. doi:10.1016/j.lfs.2020.118173
39. Tu Y, Zhu M, Wang Z, et al. Melatonin inhibits Müller cell activation and pro-inflammatory cytokine production via upregulating the MEG3/miR-204/Sirt1 axis in experimental diabetic retinopathy. *J Cell Physiol*. 2020;235(11):8724–8735. doi:10.1002/jcp.29716
40. Nicholson JK, Holmes E, Kinross J, et al. Host-gut microbiota metabolic interactions. *Science*. 2012;336(6086):1262–1267. doi:10.1126/science.1223813
41. Donald K, Finlay BB. Early-life interactions between the microbiota and immune system: impact on immune system development and atopic disease. *Nat Rev Immunol*. 2023;23(11):735–748. doi:10.1038/s41577-023-00874-w
42. Iatcu CO, Steen A, Covasa M. Gut microbiota and complications of type-2 diabetes. *Nutrients*. 2021;14(1):166. doi:10.3390/nu14010166
43. Guggenheimer J, Moore PA, Rossie K, et al. Insulin-dependent diabetes mellitus and oral soft tissue pathologies: II. Prevalence and characteristics of Candida and Candidal lesions. *Oral Surg Oral Med Oral Pathol Oral Radiol Endod*. 2000;89(5):570–576. doi:10.1067/moe.2000.104477
44. Ma K, Han Z, Sun J, et al. Mechanism of Sanhuang Decoction in alleviating DSS-induced ulcerative colitis in mice with Candida albicans colonization based on high-throughput transcriptome sequencing. *China J Chin Mater Med*. 2021;46(15):3915–3925. doi:10.19540/j.cnki.cjcmm.20210521.701
45. Dong N, Li X, Xue C, et al. Astragalus polysaccharides attenuated inflammation and balanced the gut microflora in mice challenged with Salmonella typhimurium. *Int Immunopharmacol*. 2019;74:105681. doi:10.1016/j.intimp.2019.105681
46. Mandaliya DK, Patel S, Seshadri S. Postbiotic potential of SCFAs on metaflammation and gut microbiota alteration in diabetes. *J Biosci*. 2025;50:57. doi:10.1007/s12038-025-00531-5
47. Kou B, Yu Q, Yan Y, et al. Study on the difference between combined decoction and single decoction of Danggui Liuhuang Decoction in treating yin deficiency hyperthyroidism based on network pharmacology and 16S rDNA sequencing. *Chin Tradit Herbal Drugs*. 2023;54(08):2488–2501. doi:10.7501/j.issn.0253-2670.2023.08.012
48. Charles MH, Schousboe K, Thybo T, Hall-Andersen EK, Knudsen ST. Evaluating risk stratification according to type 2 diabetes guidelines in primary care - Insights from the Danish DIAGRAM project. *Prim Care Diabetes*. 2025;19(4):368–374. doi:10.1016/j.pcd.2025.05.002